

**CNT-POLYIMIDE NANOCOMPOSITE PIEZORESISTIVE THIN FILM DEVICES
FOR STRAIN AND PRESSURE MEASUREMENT**

by

Qiuyan Li

BS, North China University of Water Resources and Electric Power, 2011

Submitted to the Graduate Faculty of
Swanson School of Engineering in partial fulfillment
of the requirements for the degree of
Master of Science

University of Pittsburgh

2015

UNIVERSITY OF PITTSBURGH
SWANSON SCHOOL OF ENGINEERING

This thesis was presented

by

Qiuyan Li

It was defended on

March 9, 2015

and approved by

William S. Slaughter, Ph.D., Associate Professor

Department of Mechanical Engineering and Materials Science

Patrick Smolinski, Ph.D., Associate Professor

Department of Mechanical Engineering and Materials Science

Thesis Advisor: Qing-Ming Wang, Ph.D., Professor

Department of Mechanical Engineering and Materials Science

Copyright © by Qiuyan Li

2015

CNT-POLYIMIDE NANOCOMPOSITE PIEZORESISTIVE THIN FILM DEVICES FOR STRAIN AND PRESSURE MEASUREMENT

Qiuyan Li, M.S.

University of Pittsburgh, 2015

In this thesis, piezoresistive thin film devices made of carbon nanotube (CNT)-polyimide (PI) nanocomposite were fabricated and characterized. Based on the percolation threshold, the CNT-PI nanocomposites with five different CNT weight ratios were chosen and made by suspension mixture method. The CNT-PI nanocomposite suspensions were deposited on the polyimide substrate by a drop-on-demand piezoelectric inkjet printer to fabricate piezoresistive thin film devices. The electrical impedance and the strain of the nanocomposite thin films under uniaxial tension and uniform pressure were characterized, and the strain sensor gauge factors were calculated. The temperature and humidity effect on the performance of the nanocomposite thin film devices were evaluated: the temperature coefficient was measured and the methods for temperature compensation were proposed; the resistance changes of the nanocomposites with humidity variation were monitored, and Parylene-C thin film coating was used to eliminate or reduce the humidity effect. The piezoresistive nanocomposite thin film devices are used for pressure measurements. Finally, the sensitivities of the CNT-PI nanocomposite of different geometrical shapes under different types of load were defined and the values of sensitivities were evaluated by experiments. The inkjet printing method showed its advantages over the traditional thin film fabrication methods for its ability to precisely control the geometry and the uniformity

of the nanocomposite thin film. The research results demonstrated that CNT-PI piezoresistive nanocomposite devices are promising candidates for flexible strain/pressure sensing applications.

TABLE OF CONTENTS

PREFACE.....	XIII
1.0 INTRODUCTION	1
1.1 INTRODUCTION	1
1.2 RESEARCH OBJECTIVES.....	3
2.0 RESEARCH BACKGROUND	6
2.1 STRAIN AND PRESSURE SENSOR.....	6
2.2 PIEZORESISTIVE MATERIALS	10
2.3 INKJET PRINTING TECHNOLOGY	12
2.3.1 Printing Technology History	12
2.3.2 Drop formation Principles of Inkjet printer	14
2.3.3 Previous Application of Inkjet printer as fabrication methods	15
3.0 PIEZORESISTIVE PROPERTY CHARACTERIZATION OF CNT-POLYIMIDE NANOCOMPOSITE DEVICES	17
3.1 INTRODUCTION	17
3.2 THEORETICAL BACKGROUND	18
3.2.1 Strain Gauge	18
3.2.2 Gauge factor and Sensitivity.....	20
3.2.3 Piezoresistive Effect.....	21
3.2.4 Percolation Theory	22

3.2.5	Equivalent circuit	23
3.2.6	Barlow's Equation and Hook's Law	25
3.2.7	Summary of testing method.....	26
3.3	NANOCOMPOSITE FABRICATION.....	27
3.3.1	Suspension Fabrication	27
3.3.2	Printing Procedure	28
3.4	CNT NANOCOMPOSITE RESPOND TO UNIAXIAL LOAD	33
3.4.1	Experimental Setup	33
3.4.2	Results and Discussions.....	35
3.5	CNT NANOCOMPOSITE RESPOND TO PRESSURE.....	36
3.5.1	Experimental Setup	37
3.5.2	Results and Discussions.....	39
3.6	CONCLUSION	45
3.6.1	Printing technique	45
3.6.2	Tensile testing and Pressure testing results comparing	46
4.0	CNT-POLYIMIDE NANOCOMPOSITES RESPONSE TO TEMPERATURE	48
4.1	INTRODUCTION	48
4.2	TEMPERATURE COEFFICIENT FACTOR.....	48
4.3	EXPERIMENT	49
4.3.1	Testing Setup and Procedure.....	49
4.3.2	Testing Results	50
4.3.3	Discussion and Conclusions	54
5.0	CNT-POLYIMIDE NANOCOMPOSITES RESPONSE TO HUMIDITY	58
5.1	INTRODUCTION	58

5.2	EXPERIMENT	58
5.2.1	Testing Setup and Procedure.....	58
5.2.2	Testing Results	60
5.2.3	Discussion and Conclusions	61
6.0	GEOMETRY EFFECT	63
6.1	SUSPENSION FABRICATION (1.8%WT CNT)	63
6.2	PRINTING PROCEDURE.....	64
6.3	FORMULA DERIVATION.....	66
6.3.1	Trapezoid.....	66
6.3.1.1	Definition for resistance.....	66
6.3.1.2	Definition for Sensitivity.....	67
6.3.2	Ring.....	68
6.3.2.1	Definition for Resistance	69
6.3.2.2	Definition for Sensitivity.....	69
6.4	SENSITIVITY CALIBRATION.....	71
6.4.1	Results and Discussions.....	71
7.0	CONCLUSIONS.....	73
7.1	PRINTING ADVANTAGES	73
7.2	CONCLUSIONS AND FUTURE WORKS.....	75
	BIBLIOGRAPHY	78

LIST OF TABLES

Table 3.1 Voltage Wave Parameter [45].....	29
Table 3.2 Strain on substrate corresponding to Pressure	42
Table 4.1 Temperature Coefficient Summary	57
Table 6.1 Suspension Fabrication	64
Table 7.1 Comparison of Different thin film Fabrication Methods.....	73

LIST OF FIGURES

Figure 2.1 Strain gauge principle [16]	6
Figure 2.2 Basic rosette types classified by grid orientation (a) tee; (b) 45°-rectangular; (c) 60°-delta [18]	8
Figure 2.3 Rectangular rosettes (of the same gauge length) in planar and stacked construction [18].....	8
Figure 2.4 Elastic elements used as pressure sensor [15]	10
Figure 2.5 Micro Measurements diaphragm strain gauges for pressure transducers [19]	10
Figure 2.6 Classification of inkjet printing technology [34].....	12
Figure 2.7 Classification of piezoelectric inkjet printhead actuation principles [33]	14
Figure 3.1 Rectangular Resistance.....	18
Figure 3.2 Tunneling effect model [44]	22
Figure 3.3 Conductivity of CNT nanocomposites with different weight ratio [6]	23
Figure 3.4 Equivalent circuit of the CNT nanocomposites thin film.....	24
Figure 3.5 Cole-Cole Plot	25
Figure 3.6 Inkjet Printing Station and the operation software [46]	30
Figure 3.7 Wave form of drop formation, drop generation procedure and the picture of generated drops of CNT-PI suspension [46]	31
Figure 3.8 Pattern and Sample printing procedure	32
Figure 3.9 Sample photo	34

Figure 3.10 Testing equipment (stress/strain apparatus (left) and current/voltage source measure unit (right)).....	35
Figure 3.11 Normalized resistances with strain of CNT concentration from 1.2wt% to 2.0%	35
Figure 3.12 Summary of Gauge factor	36
Figure 3.13 Sample photo.....	37
Figure 3.14 Testing Equipment.....	38
Figure 3.15 Impedance of test sample with CNT concentration of 1.2wt%	39
Figure 3.16 Impedance of test sample with CNT concentration of 1.4wt%	40
Figure 3.17 Impedance of test sample with CNT concentration of 1.6wt%	40
Figure 3.18 Impedance of test sample with CNT concentration of 1.8wt%	41
Figure 3.19 Impedance of test sample with CNT concentration of 2.0wt%	41
Figure 3.20 Resistance change with strain of the five nanocomposites	42
Figure 3.21 Gauge factor/sensitivity of resistance summary.....	43
Figure 3.22 Capacitance change with strain of the five nanocomposites.....	43
Figure 3.23 Gauge factor/Sensitivity of Capacitance summary	44
Figure 4.1 Hotplate for temperature control	50
Figure 4.2 Impedance of test sample with CNT concentration of 2.0 wt% with respect to frequency	51
Figure 4.3 Impedance of test sample with CNT concentration of 2.0wt%	51
Figure 4.4 Impedance of test sample with CNT concentration of 1.8wt%	52
Figure 4.5 Impedance of test sample with CNT concentration of 1.6wt%	52
Figure 4.6 Impedance of test sample with CNT concentration of 1.4wt%	53
Figure 4.7 Impedance of test sample with CNT concentration of 1.2wt%	53
Figure 4.8 Resistance change with temperature of CNT nanocomposites with different CNT concentration	54

Figure 4.9 Normalized Temperature Coefficient for CNT nanocomposites with different CNT concentration	55
Figure 5.1 Chamber Setup	59
Figure 5.2 Normalized Resistances response to Humidity	60
Figure 5.3 Normalized Resistance respond to Humidity with Parylene Coating	61
Figure 6.1 Photos of Sample	65
Figure 6.2 Trapezoid	66
Figure 6.3 Sector and Ring	68
Figure 6.4 Impedance of Ring Shaped Transducer.....	71
Figure 6.5 Sensitivity Summary	72
Figure 7.1 Photos of printed sample	75

PREFACE

I am so grateful that I have so many nice people around supporting and encouraging me during my thesis work.

First, I would like to express my sincerest appreciation to my thesis advisor, Dr. Qing-Ming Wang, for giving me this opportunity to work on this topic and for all of his encouragement, support and guidance during this research and over the past three years of my M.S. study. I am very thankful to Dr. William S. Slaughter and Dr. Patrick Smolinski for their kindly willingness to serve as my committee members and their helpful suggestions.

Meanwhile, I would like to thank my colleagues: Hongfei Zu, Huiyan Wu, and Rongjie Liang for their help in my research, and my friends Lina Xu and Lan Xing for their encouragement.

Finally, I would like to express my deepest gratitude to my families who are always supporting me and loving me.

1.0 INTRODUCTION

1.1 INTRODUCTION

Strain sensor has been widely used in numerous industrial, civil, medical and aerospace fields [5]. And strain measurement is essential for many other physical quantities measurements. For example, stress can be determined from strain based on solid mechanics principles, and indirect measurements of force, pressure and temperature can also be achieved by strain measurement [1].

There are various kinds of techniques to measure the strain or displacement response in a mechanical structure, and they can be grouped into either noncontact or contact methods [2]. Typical noncontact methods are laser strain micrometry and optical microscope, where laser strain micrometry use laser beam reflection to characterize the transverse strain response of a structure [3], and optical microscope can only be used at low frequency response region [4]. Contact methods include resistive strain gauge, differential capacitive strain gauge and linear variable differential transformer (LVDT) [5]. The differential capacitive strain gauge measures the output voltage of two differential parallel plate capacitors, and the LVDT measures the output voltage of two differential transformers, both use the voltage output to reflect the structure displacement change. The electrical resistance strain gauge is the most common transducer to measure strain. In order to measure the strain of a mechanical component, the resistance strain

gauge is usually attached on the component directly, and once the component is loaded, the gauge is also deformed and the strain of the component can be determined by the accurately measured resistance change of the gauge [1]. Resistance strain gauges use metal foil or piezoresistive semiconductor thin film to characterize static or dynamic strain variations. Most metal strain gauges have gauge factor between 2 and 5, and they are rigid which makes them not suitable for small flexible deformation measurement [6]. Polymer based piezoresistive nanocomposites, on the contrary, have shown better structural flexibility and higher gauge factor [5][6][7][8]. In sum, piezoresistive nanocomposite strain gauge is good candidate for tactile strain sensing and pressure testing.

Several methods have been used for fabricating the thin film of nanocomposites, like spin coating method for ZnO- polyimide (PI) nanocomposites [5] and manually painting using transfer pipe for single wall Carbon nanotube (swCNT)-PI nanocomposites [6]. By introducing inkjet printing method, the geometry of the transducer thin film can be better controlled and the uniformity of the thin film can be improved. There are a lot of nanocomposite materials whose piezoresistive properties have been studied, like ZnO-PI [5], swCNT-PI [6], CNT-Epoxy [7] and CNT-PMMA [8]. In this research, swCNT-PI nanocomposite is chosen. Based on some previous research [6], the viscosity of the swCNT-PI suspension is relative low that generating the drops during inkjet printing is easier.

In this thesis, swCNT-PI nanocomposites with different CNT weight ratio were fabricated, and then printed on the polyimide substrate. The piezoresistive property of the nanocomposites was investigated and then the nanocomposite with the best sensitivity was found. The possible temperature and humidity effect on the performance on the nanocomposite sensors were considered, and the compensation methods were proposed. Depending on the

complexity of the application requirement, more precise definitions of sensitivity of sensors with different shape and types of load were derived, and the sensitivity of the swCNT-PI nanocomposite strain/pressure sensor was obtained through experiments.

1.2 RESEARCH OBJECTIVES

The objective of this study is to demonstrate that Carbon Nanotube-Polyimide Nanocomposite is a good candidate as transducer in a strain/pressure sensor and that inkjet printing method is a viable processing method to fabricate the transducer thin film. To achieve this goal, three research tasks will be performed in this study: fabricate the nanocomposite thin film using inkjet printing method; characterize the strain sensing performance of the nanocomposite thin film transducer when force or pressure is applied; evaluate the temperature effect on the transducer and determine the temperature coefficient of the piezoresistive nanocomposite devices; and finally evaluate the humidity impact on the transducer, and study the performance of Parylene coating to eliminate effect of humidity.

- **Fabrication the CNT-Polyimide nanocomposite thin film using inkjet printing method:**

Previous work on the CNT-Polyimide thin film devices used spin coating method to deposit thin layer of nanocomposite on silicon substrate [5], or manually paint the nanocomposite slurry on the plastic substrate [6] for device fabrication. Using small brush to paint a thin layer CNT-Polymer nanocomposites was found to be inconsistent in device fabrication thought it is a very simply approach. Compared to these methods, inkjet printing method has shown advantages in the fabrication of functional materials and devices [10][11][12].

Inkjet printing fabrication of devices would offer some unique advantages including fast-prototyping of functional devices, easy control of the geometrical shape of devices and good uniformity of the material components deposited.

- **Gauge factor/Sensitivity evaluation of CNT-Polyimide nanocomposite:**

Gauge factor/sensitivity is the most important parameter for the evaluation of piezoresistive device. Gauge factor is defined as the relative resistance change per unit longitudinal strain ($\frac{\Delta R}{R}/\epsilon$). Large gauge factor is always preferable for high sensitive strain sensing applications. In the experimental study, two loading methods will be applied to the specimen on which the CNT/Polymer nanocomposite devices is fabricated to assess the gauge factors: uniaxial tension and pressure. And two electric testing methods will be used to find the electric resistance change verse the applied mechanical strain: DC resistance measurement and AC electrical impedance spectroscopy measurement for CNT/polymer nanocomposite sensors under different strain levels. The electrical impedance spectroscopy measurement allows the extraction of equivalent DC resistance at very low frequency range, and the equivalent capacitance at a characteristic frequency of the of the piezoresistive nanocomposite device.

The deformation of the thin film of different shape under different kind of load would vary, and the mathematical definition of sensitivity would be different from the Gauge factor definition, the specific definition and the values of the sensitivity of trapezoid and ring shaped thin film need to be studied.

- **Measurement of temperature coefficient of nanocomposite piezoresistors and evaluation of the humidity effect on the device performance:**

Temperature and humidity are two major factors that would interfere the performance of the piezoresistive nanocomposite strain sensors. In this study, the temperature coefficient of the

nanocomposite strain sensor will be characterized. For the compensation of temperature effect, it is suggested that a dual sensor configuration will be applied when the device is applied to strain measurement. In a previous research work, Parylene-C coating has been shown to be an effective packaging material to eliminate the humidity effect in acoustic wave gas sensor [9]. In this work, the same strategy will be used to reduce the potential humidity effect of the CNT/polymer piezoresistive strain sensor. How the nanocomposite strain sensor could respond to humidity will be examined systematically by monitoring the resistance change at different humidity levels. The electrical resistance of the same group of devices will be tested again after Parylene thin film is coated on the surface to show if the Parylene coating layer can effectively eliminate and substantially reduce the humidity effect on the strain gauge.

2.0 RESEARCH BACKGROUND

2.1 STRAIN AND PRESSURE SENSOR

The electrical resistance strain gauge is the most common used strain transducer. It was invented by Edward E. Simmons and Arthur C. Ruge in 1938 [13][14]. The strain gauge usually consists a strain sensitive thin film made of metal or semiconductor material and an insulating backing carrier of the thin film. The principle of the strain gauge is based on the fact that the electrical resistance of the metal or semiconductor thin film would change if the thin film deforms [15]. The resistance strain gauge also forms the basis for a variety of other transducers like load cells, pressure transducers and torque meters [15].

There are two types of working principles of the strain gauge: extension and compression. For extension gauges, the strain gauge is elongated and cross section area narrows, so the resistance would increase under the load; while for compression gauges, the resistance decreases [1].

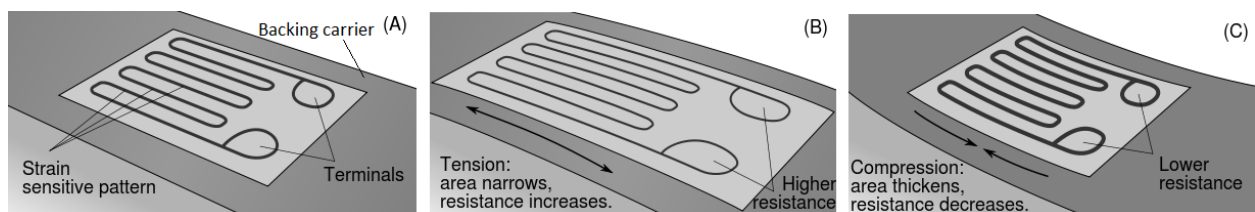


Figure 2.1 Strain gauge principle [16]

Different configurations of strain gauge have been invented to meet the complex requirements for different types of strain, stress and pressure measurement. This includes strain gauge rosettes for strain on different direction and diaphragm strain gauges [17][18][19][20]. Figure 2.2, 2.3 and 2.5 show some of the configurations. The original single grid gage could only be used when the stress at the point of measurement is known to be uniaxial and the directions of the principal axes are known in experimental stress analysis. Due to the limitation of the single grid gauge, strain gauge rosettes were invented to measure the biaxial stress states. By definition, a strain gauge rosette is an arrangement of two or more closely positioned gauges, which are oriented separately to measure the normal strains along different directions in the surface of the test part [18]. The configuration of strain gauge rosettes is described by rosette type and rosette constructions. Three basic types of strain gauge rosettes are shown in figure 2.2: the two elements 90-degree or tee rosette (a), which can be employed when the principal strain directions are known in advance and cylindrical pressure vessels and shafts in torsion are typical examples; the three elements (b) and (c), which can be used in more general cases when the directions of the principal directions of the surface stress is uncertain [17]. All three types of rosettes can be manufactured in both planar and stacked versions, where planer construction gives minimal reinforcing effect and better heat dissipation to the test part while stacked construction can be installed on small spaces where its planar counterpart couldn't be fit in [18].

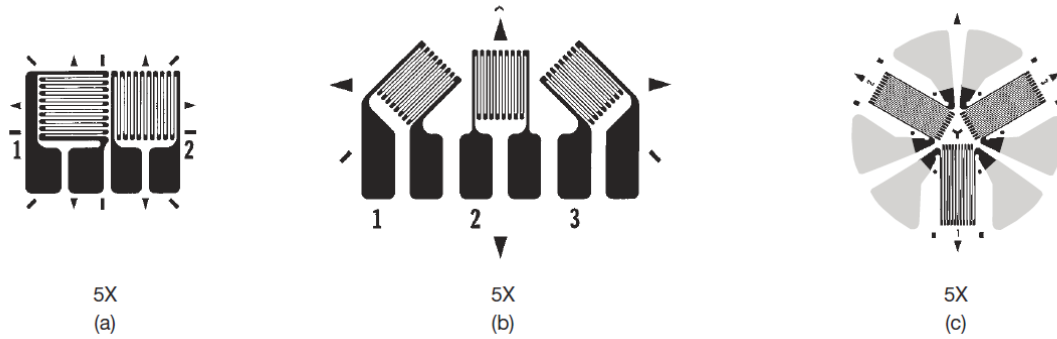


Figure 2.2 Basic rosette types classified by grid orientation (a) tee; (b) 45°-rectangular; (c) 60°-delta [18]

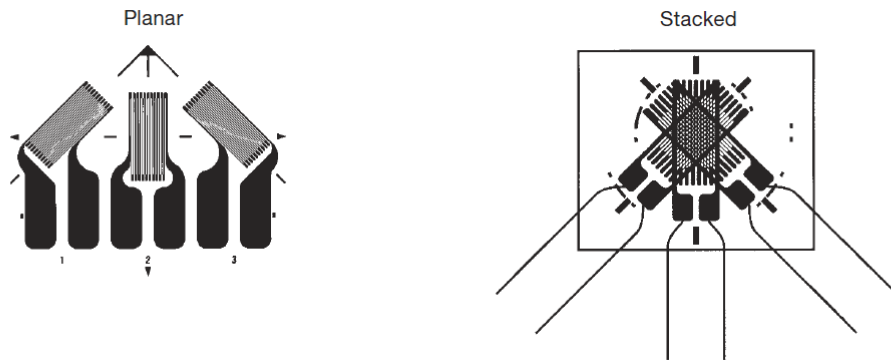


Figure 2.3 Rectangular rosettes (of the same gauge length) in planar and stacked construction [18]

The traditional strain gauge is metallic strain gauge, who use zigzag grid of thin foil bonded on the substrate like which are shown in figure 2.2-2.4. The typical gauge factors for metallic strain gauge are from 2 to 5 [1]. The other type of element used for strain gauge is semiconductor, who also exhibits a change in resistance under load. Comparing to metallic strain gauge, the semiconductor gauge exhibits very large gauge factor 5-200, and exhibits higher resistance, longer fatigue life, and lower hysteresis under some conditions [15]. Using semiconductor materials, the strain gauge can be more flexible than metallic strain gauge. However, the strain sensitivity of the semiconductor strain gauge is easier affected by

temperature [15]. For resistance strain gauge, piezoresistive materials are common used among semiconductor materials.

Wheatstone bridge is often used as the circuit for resistance changes of strain gauge measurement. Though, there are several variations of Wheatstone bridge for different applications, the configuration of the Wheatstone bridge is similar: there are four resistors that connected in a loop to form a basic bridge, and one of the resistor is the strain gauge which is a potentiometer (variable resistor). Input voltage is applied across two junctions and the output voltage the other two junctions. When the resistance of the stain gauge changes and output voltage would change with it, comparing the voltage change with the original value the resistance change and the strain can be calculated.

A pressure sensor converts a measured pressure into a mechanical or electrical signal [15]. A pressure transducer consist a primary sensor and a secondary sensor. The primary sensor is an elastic element who deforms or deflects under pressure, and the common elastic elements are shown in figure 2.4: Bourdon tube is a curved metal tube with an elliptical cross section that deforms with the pressure difference between the outside and inside the tube; the bellows and the capsule sensing elements are thin walled flexible metal tubes, the length of which changes with the variation of difference between external and internal pressure; a diaphragm is a thin elastic circular plate supported about its circumference, and the deformation of the diaphragm is proportional to the pressure difference [15]. Strain gauge elements, capacitance elements and piezoelectric crystal elements are typical secondary elements which converts the deflection of the elastic elements into a measureable signal like electrical voltage or mechanical rotation [15]. Piezoelectric crystal elements are effective elements for dynamic pressure measurement; capacitance elements can be created when a fixed metal plate is placed above or below a metallic

diaphragm; and a strain gauge can be bonded directly on the diaphragm. Figure 2.5 shows two industrialized patterns of strain gauge diaphragm for pressure sensing.

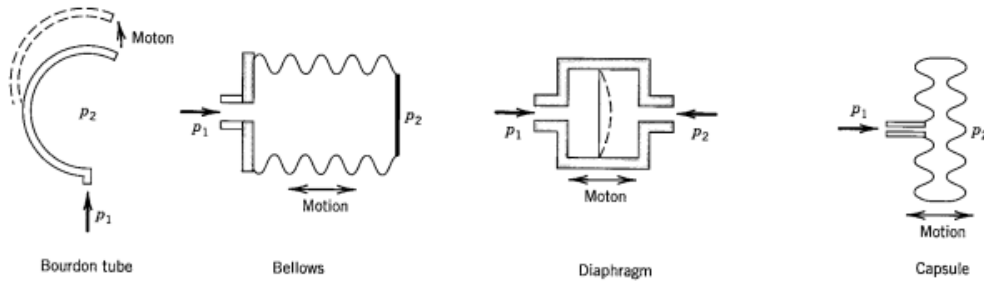


Figure 2.4 Elastic elements used as pressure sensor [15]

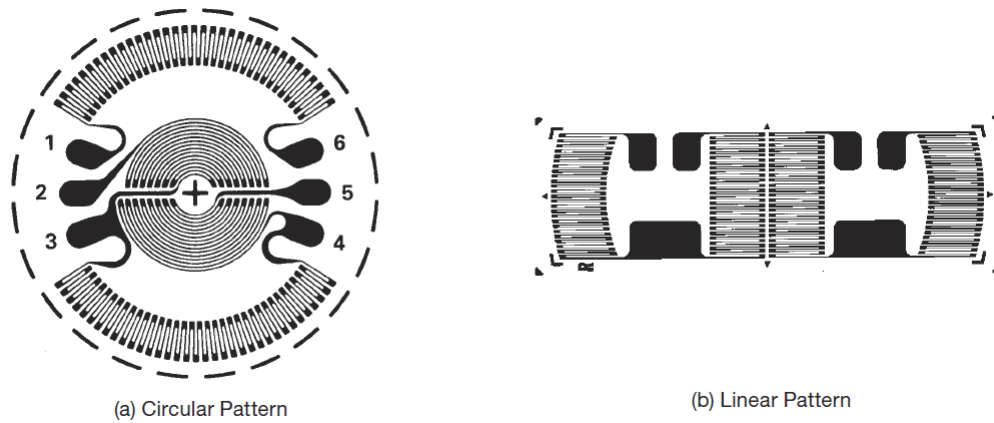


Figure 2.5 Micro Measurements diaphragm strain gauges for pressure transducers [19]

2.2 PIEZORESISTIVE MATERIALS

Piezoresistive strain gauges can use single crystal silicon and polycrystalline silicon as the transducer element. However, polymer matrix nanocomposites are becoming a set of materials for piezoresistive strain sensing especially for small strain and flexible sensing, due to their structural flexibility and the possibility of combining multiple function. A giant

piezoresistive effect has been observed in silicon nanowires [21]. Piezoresistive properties of crystalline and polycrystalline silicon nanowires have been investigated [22]. ZnO nanowires have been investigated in the past few years [23]. The electrical and mechanical properties of carbon nanotubes and the piezoresistive property of carbon nanotube-polymer nanocomposites have been studied for strain sensor utilization [24][25].

The widely used nano-scale carbon filler particles for nanocomposite strain sensors are swCNT [6][26], mwCNT [7][8][27], carbon nanofibers [29], carbon nanoblacks [28] and graphene [30]. The influence of the type of nano scale filler on the piezoresistivity of the sensor is significant [31]. And the insulating polymer matrices, like epoxy [8], PMMA [7], EMMA [27], PE [26][27], and PI [5][6] etc., have small influence on the piezoresistivity, and the only significant influence is that the viscosity of the nano-filler polymer suspension would vary depending on the different type of polymer and that would determine the characteristics of the mixing and dispersing process [31]. Previous researches show that the gauge factor of ZnO-PI nanocomposite can reach to 100 [5]. And a lot of researches have been done on the piezoresistive CNT-polymer nanocomposite strain sensors, for example, Hu et al reported the gauge factor of mwCNT-Epoxy can reach to 20~25 under maximum strain of 0.006 [8], Loh et al made swCNT-PE with sensitivity of 0.1~0.8 [26], Kang et al reported mwCNT-PMMA has gauge factor of 5 with maximum strain of 0.0015 [7], and gauge factor of swCNT-PI from Wang et al is 5 and the max strain is 0.02 [6]. Besides, polyimide has better thermal stability and mechanical properties [32].

Generally, CNT-Polymer nanocomposites do not have the larger sensitivity comparing to some other nanotube/nanowire-polymer nanocomposites. However, the broad strain testing range which decided by the good mechanical property of CNT and the easiness of fabricating the

nanocomposite still make it a good candidate for fabrication the thin film by innovated fabricating method for strain and pressure testing.

2.3 INKJET PRINTING TECHNOLOGY

2.3.1 Printing Technology History

Though the first inkjet like device was invented by William Thomson in 1858, the rapid development of this technology started off at late 1950s [33]. There are several kinds of inkjet printing technology has been developed since then, and the classification is shown in Fig. 2.1, and among them piezoelectric and thermal inkjet are the dominants in this field.

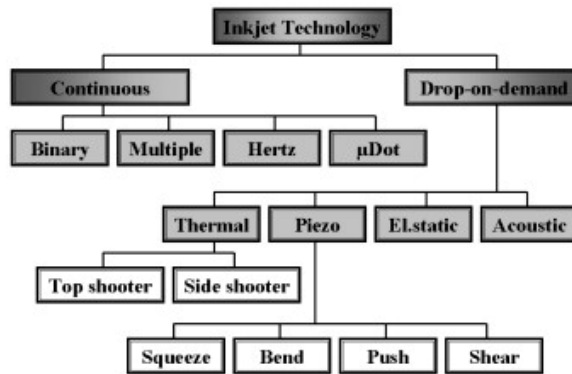


Figure 2.6 Classification of inkjet printing technology [34]

Continuous Inkjet printing (CIJ) emerged in early 1960s was elaborated for inkjet bar coding in Stanford University. By applying a pressure wave pattern to the print head orifice, the ink stream can be broken into droplets of uniform size and spacing [35]. With this controlled jet break up mechanism, the drops could be charged selectively as they emerged out the continuous jet and the charged drops were deflected towards several positions to form an image on the

substrate when passing through an electric field, while the uncharged drops can be captured by the re-circulated system. The A.B. Dick Company made the first commercial CIJ product in 1968, and then Sharp, IBM, Honeywell developed their own licensed technology with further development of multiple drop defection, increased drop frequency, and multi-jet printing respectively [33].

Instead of firing drops continuously, it is also possible to create drops only when an actual pulse is provided, which is called drop-on-demand (DOD) technique. The DOD technique is much more widely used than CIJ majorly because there is no need to use the complicated hardware for charging electrodes, deflecting electrodes and re-circulation system [33]. The first DOD technique also emerged in 1960s. For a DOD printhead, the ink is held in the nozzle by a negative pressure and by applying a high voltage pulse to electrodes located outside the nozzle, a drop of ink is pulled out by the deflection of the nozzle [36]. Among the four DOD printing techniques, the piezoelectric inkjet printing and thermal inkjet printing are the two most important printing technique at present.

The basic idea about thermal inkjet printing was brought up in 1960s, which is a drop of ink could be generated by boiling aqueous ink at certain time instances. But the idea was abandoned until Canon and HP picked it up. In 1979, Canon re-invented the DOD printhead called bubblejet which is actuated by a water vapor bubble, and the droplet was ejected in a perpendicular direction from the evaporating bubble. While HP introduced its low cost inkjet printer called top shooter design with jetting direction in line with the evaporating bubble in 1984 [33].

Another DOD technique is called piezoelectric inkjet (PIJ), which use a piezo electrical unit to convert an electrical driving voltage into a mechanical deformation of the ink chamber to

generate the pressure required for the drop formation from the nozzle [33]. There are several patents in 1970s and 1980s that contribute the development of this technology. First squeeze mode PIJ was proposed by Zoltan of Clevite Company in 1972 [37]. A hollow tube of piezoelectric material is used and the ink chamber would be squeezed and force out a drop when a voltage is applied on the material [37]. In 1973, a bend mode of operation was used in patent of Stemme of Chalmers University, and the wall of the ink chamber is made of a diaphragm bonded with a piezoelectric ceramic which would bend under voltage [38]. Kyser et al. patented similar bending mode PIJ with different shape of actuation plate in 1976 [39]. S. Howkins of Exxon in 1984 described the push mode (or bump mode) operation where a piezoelectric element pushes against an ink chamber wall to deform the ink chamber and the electrical field is applied in the poling direction and the deformation is in the same or perpendicular direction to the poling direction [33]. Finally, the shear mode was proposed by Fischbeck, where the electric field is perpendicular to the poling direction of the piezoelectric ceramic [33]. Till then, the commonly adapted categorizations of PIJ have all been introduced.

2.3.2 Drop formation Principles of Inkjet printer

After a brief historical review on inkjet printing technology, the principles of the piezoelectric inkjet printer and different actuation principle will be briefly summarized in this section.

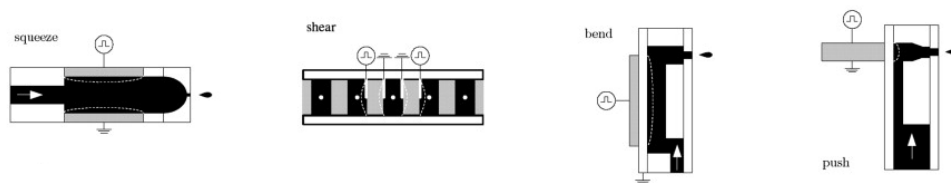


Figure 2.7 Classification of piezoelectric inkjet printhead actuation principles [33]

The driving force of a piezoelectric inkjet printhead is driven by this ‘inverse piezoelectric effect’, where the structure of the material would be deformed when an external electric field is applied. And there are three major modes of actuation: bump, bend and shear mode as it is introduced in the previous section. A bump mode actuator has the actuation movement directed along the polarization of the piezoelectric material, and in order to deform an ink channel, the piezoelectric elements need to be supported by a substrate which supplies the reaction force. The substrate would introduce mechanical stress and the piezoelectric behavior would be influenced. While bending mode actuators bend the complete channel wall or part of channel wall which are made of piezoelectric materials themselves. In both bump mode and bend mode actuation, electric field is applied in the same direction as the polarization direction. Shear mode actuators use electric field applied perpendicular to the polarization direction which result in a shear deformation parallel to the polarization direction [33].

2.3.3 Previous Application of Inkjet printer as fabrication methods

As reviewed in the previous sections, inkjet printing technique has been developed a major fabrication method to print text and images onto papers and other porous surfaces [33]. While in the recent few decades, it has been developed to be used as a fabrication method for fabricating electrical mechanical devices with different kinds of materials [40].

Kaydanova et al. used direct write inkjet printing to fabricate tunable circuits [41]. This circuit is made of BST films, which is deposited on MgO substrate by using MicroFab MikroJet to print this solution (BST). The printhead was driven by a computer-controlled wave form generator with a frequency of 20 kHz and multiple layers were printed for thicker films.

Van Osch et al. DOD inkjet printing conductive tracks on polymeric substrates [42]. A silver ink with 20wt% silver nanoparticles suspended in ethylene glycol/ethanol mixture was inkjet printed on transparent polyarylate film performed by using a piezoelectric Dimatix DMP 2800 (Fuji film). The printhead contained 16 parallel squared nozzles and the suspension was printed at 16 V, a 5 kHz frequency and a customized wave form, and the substrate heated to 60°C.

Rausch et al. printed piezoresistive strain sensors with the combination of using screen printing and inkjet printing [43]. Steel is used as substrate in their research, so an insulating layer between sensing layer and the substrate is built by screen print polyester resin on the substrate. Two sensing layers were used: first one which is made by thermally cross-linking silver suspension was screen printed on the insulating layer. The second layer was inkjet printed by PEDOT: PSS a conductive polymer water based suspension by a Dimatix inkjet printer (Fuji Film).

3.0 PIEZORESISTIVE PROPERTY CHARACTERIZATION OF CNT-POLYIMIDE NANOCOMPOSITE DEVICES

3.1 INTRODUCTION

Piezoresistive materials have long been used as the transducer elements for pressure or strain testing. The piezoresistive strain gauge has a larger gauge factor, which will be discussed later, to be a parameter to qualify sensitivity of a strain sensor. Many semi-conductive materials have been studied as candidates for strain sensor. In this research, single wall carbon nanotube-polyimide nanocomposite is the object.

In this chapter, the piezoresistive property of the carbon nanotube nanocomposite will be studied. The background theory will be reviewed first, followed by the experimental setup and procedure. Starting at the concept of strain gauge, definition of gauge factor, piezoresistive effect, and percolation theory, the background knowledge is built up. Then an equivalent circuit of the nanocomposite transducer is then presented which not only represents the electrical property of the nanocomposite thin film, but also shows which parameters should be tested during experimental study to investigate the electrical properties of the nanocomposite.

The carbon nanotube (CNT) polyimide nanocomposites with a series of CNT weight ratios are fabricated, and then inkjet printing processing is applied to deposit thin film devices on a polyimide substrate. Prior to the deposition, interdigitated transducer (IDT) electrodes are

formed on the substrate by depositing a gold thin film using shadow mask and a sputter coating system. Once the nanocomposite thin film device has been printed and baked in the oven, the nanocomposite strain sensors are ready to be tested.

Two loading methods are applied to the specimens on whom the CNT/Polymer nanocomposite devices are fabricated to assess the piezoresistive gauge factors: uniaxial tensile loading and uniform pressure loading. Both electrical impedance spectroscopy and DC electrical resistance measurement are used to show electrical property of the nanocomposite thin film devices. The electrical properties can be analyzed based on the testing results. The optimal weight ratio of CNT to polymer matrix in the nanocomposite devices with high gauge factor can be concluded.

3.2 THEORETICAL BACKGROUND

3.2.1 Strain Gauge

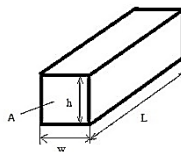


Figure 3.1 Rectangular Resistance

A rectangular conductor is illustrated in figure 3.1, whose resistance is given by

$$R = \frac{\rho L}{A} \quad (3.1)$$

where ρ, L and A are the resistivity of the material, the total length and the cross-section area of the conductor respectively.

By taking the natural logarithm on both sides of Equation (3.1),

$$\ln R = \ln \rho + \ln L - \ln A \quad (3.2)$$

Then take the derivative to get

$$\frac{dR}{R} = \frac{d\rho}{\rho} + \frac{dL}{L} - \frac{dA}{A} \quad (3.3)$$

Given $A = wh$, $\frac{dA}{A} = \frac{w \cdot dh + h \cdot dw}{wh} = \frac{dh}{h} + \frac{dw}{w}$ and the definition of Poisson's ratio

$$\nu = -\frac{d\varepsilon_{trans}}{d\varepsilon_{axial}},$$

$\frac{dh}{h} = -\nu \frac{dL}{L}$ and $\frac{dw}{w} = -\nu \frac{dL}{L}$. We have

$$\frac{dA}{A} = -2\nu \frac{dL}{L} = -2\nu \varepsilon_{axial} \quad (3.4)$$

Substitute (3.4) into (3.3) to have

$$\frac{dR}{R} = (1 + 2\nu) \varepsilon_{axial} + \frac{d\rho}{\rho} \quad (3.5)$$

Finally,

$$\frac{dR/R}{\varepsilon_{axial}} = 1 + 2\nu + \frac{d\rho/\rho}{\varepsilon_{axial}} \quad (3.6)$$

On the right hand side, the first two terms represent the resistance change caused by the variance in geometry which includes the increase in length and the decrease in cross section area. The last term represents the piezoresistive property of the material, which indicates the resistivity change with strain.

3.2.2 Gauge factor and Sensitivity

The gauge factor of a material is defined as

$$GF = \frac{dR/R}{\epsilon_{axial}} \quad (3.7)$$

The gauge factor shows the relationship between the resistance change and the deformation of the material when uniaxial load is applied. The gauge factor for a metallic strain gauge is dominated by the geometry terms and the gauge factor of piezoresistive gauges is dominated by the last term of equation (3.6). For a specific material, the gauge factor remains constant, and this makes it a good candidate for strain testing. Acting as strain sensor, the gauge factor of the material of the transducer represents the sensitivity of the sensor. The strain and force or pressure obey linear relationship which shows the mechanical property of the material, so the larger the gauge factor, the electric signal obtained by get the resistance change would be larger with small strain.

3.2.3 Piezoresistive Effect

Piezoresistive effect refers to the phenomenon of some material that the resistivity of the material changes with strain. From Equation 3.6, the last term on the right hand side ($\frac{dp/p}{\epsilon_{axial}}$) shows how piezoresistive effect affects resistance.

The resistance change with strain of most metal is dominated by the geometry changes which for instance is increased length and decrease in cross section area in tension. While in semiconductor materials, it could be dominated by the $\frac{dp/p}{\epsilon_{axial}}$ term, and it can be several orders larger in magnitude than the resistance change due to geometry effect. And this is the reason that why semiconductor's usage in strain gauges has been draw so many attentions in recent years.

Both piezoresistive effect term and geometry term in Equation 3.6 are approximately constant during operation range. So there exist a linear relationship of resistance change with strain and it could be represented by gauge factor (GF) defined in the previous section.

In molecular scale, the piezoresistive effect can be explained by two reasons. One is about bandgap, when semi-conducting material is subjected to force and strain occurs, there will be changes in inter-atomic spacing which makes it easier or harder for electrons to be raised in to the conduction band. For instance, when extension applied on the carbon nanotube, it is harder for electrons to go to conduction band because the inter-atomic spacing grows, and resulting in larger resistance based on this theory. The other is tunneling effect. The tunneling resistance between two neighboring CNTs can be approximated as [44]:

$$R_{tunnel} = \frac{V}{AJ} = \frac{h^2 d}{As^2 \sqrt{2m\lambda}} \exp\left(\frac{4\pi d}{h} \sqrt{2m\lambda}\right) \quad (3.8)$$

J —tunneling current density, V —electrical potential difference, e —the quantum of electricity, m —mass of electron, h —Planck’s constant, d —the distance between CNTs, λ —the height of barrier and A —cross section of the tunnel.

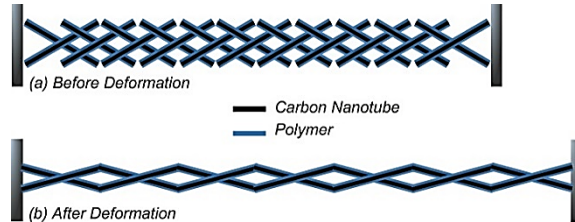


Figure 3.2 Tunneling effect model [44]

When it is subjected to extension for instance, the contacted CNT would be separated; it may introduce the tunneling resistance and make the overall resistance increases. The resistance change with strain may get contribution from the both reasons addressed above.

3.2.4 Percolation Theory

Composites containing conduction fillers in insulating polymers become electrically conductive when the filler content exceeds a critical value, known as percolation threshold. The percolation threshold is characterized by a sharp jump in the conductivity by many orders of magnitude. The sharp jump is attributed to the formation of a three dimensional conductive network of the fillers within the polymer matrix. Percolation threshold is determined by plotting the electrical conductivity as a function of the mass fraction of the conductive filler.

Based on the theory stated above, by making the carbon nanotube polyimide nanocomposite with different weight ratio of carbon nanotube, the conductivity of the composite will increase as the weight ratio of the conductor increases. Percolation formula is given by

$y = c(x - a)^b$, where x is the concentration of CNT, a is the percolation threshold, b is the critical exponent and c is a constant. By making this plot, the percolation threshold of the nanocomposites can be found.

Locating the percolation threshold is critical in this research, because the concentrations of CNT of the research should around it where the materials are semiconductors.

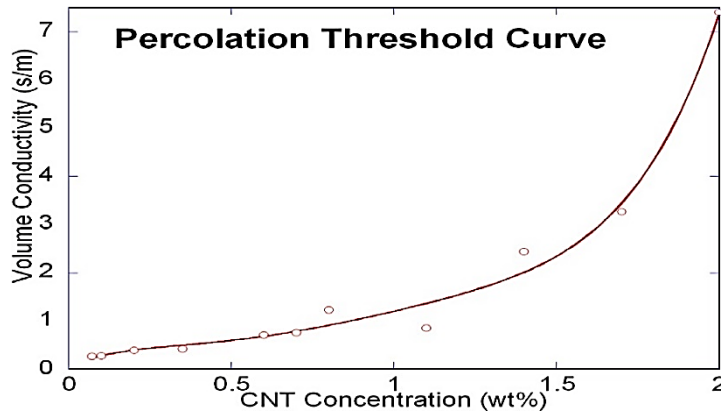


Figure 3.3 Conductivity of CNT nanocomposites with different weight ratio [6]

Based on the results from Wang et al [6], which is given by the figure 3.3, the percolation threshold should be between 1% to 2%wt. so the CNT weight ratio of 1.2%, 1.4%, 1.6%, 1.8% and 2.0% are to be studied in the research, and the electrical properties of samples with the weight ratios will be further studied.

3.2.5 Equivalent circuit

The equivalent circuit of the nanocomposite thin film can be expressed as a resistor connects with a capacitor in parallel and then connect with a resistor in series [5].

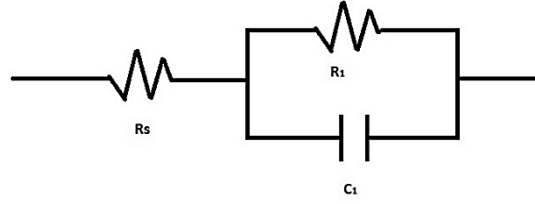


Figure 3.4 Equivalent circuit of the CNT nanocomposites thin film

The impedance of this model can be derived as follows:

Complex impedance in Cartesian form is given by $Z = R + jX$, where R (Resistance) is the real part and X (Reactance) is the imaginary part. Also, the impedance of resistor and capacitor are given by $Z = R$ and $Z = \frac{1}{j\omega C}$.

Based on the equivalent circuit, the total impedance of the thin film Z is

$$\begin{aligned}
 Z &= R_s + \frac{1}{\frac{1}{R_1} + j\omega C_1} \\
 &= R_s + \frac{R_1}{1 + j\omega R_1 C_1} \\
 &= R_s + \frac{R_1(1 - j\omega C_1 R_1)}{1 - (-1)\omega^2 C_1^2 R_1^2} \\
 &= \left(R_s + \frac{R_1}{1 + \omega^2 C_1^2 R_1^2} \right) - j \frac{\omega C_1 R_1^2}{1 + \omega^2 C_1^2 R_1^2}
 \end{aligned}$$

So

$$Z = \left(R_s + \frac{R_1}{1 + \omega^2 C_1^2 R_1^2} \right) - j \frac{\omega C_1 R_1^2}{1 + \omega^2 C_1^2 R_1^2} \quad (3.8)$$

The R-X relationship is a semicircle as frequency goes from 0 to infinity. More specifically, when $\omega \rightarrow 0$, $Z = R = R_s + R_1$; when $\omega \rightarrow \infty$, $Z = R_s$; and $\omega_0 = \frac{1}{C_1 R_1}$ at the top of the semicircle. So to evaluate these parameters, the Cole-Cole Plot shall be made.

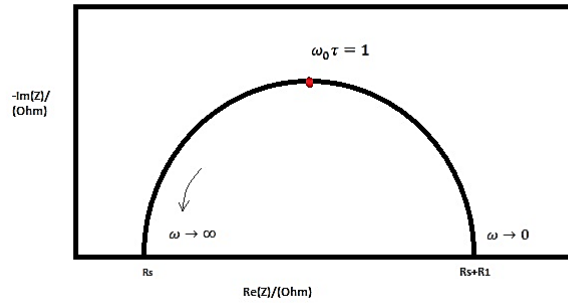


Figure 3.5 Cole-Cole Plot

3.2.6 Barlow's Equation and Hook's Law

The linearized Hook's Law relates the stress and strain, which is given by

$$\sigma = E \cdot \epsilon \quad (3.9)$$

Where E is the Young's modulus, and it is 2.5 GPa (362600 psi) for the polyimide substrate which is used in the research.

Barlow's Equation will be used when pressure testing is conducted, and it is used to relate pressure to the stress on the substrate. It is given as

$$P = \frac{2\sigma t}{d \cdot SF} \quad (3.10)$$

Where P is pressure, σ is stress, t is the thickness of the substrate, d is the diameter of the vessel and SF is the safety factor. For the polyimide substrate that is used in this research, $t=0.005$ inches. The pressure vessel will be used has an inner diameter (d) of 2 inches, and the safety factor would be chosen as 1.5.

3.2.7 Summary of testing method

To measure the piezoresistive property, there are strain to be generated and the resistance to be measured. There are lots of methods to generate the strain: tensile tester to generate uniaxial load, cantilever beam can be used to generate static and dynamic strain, and pressure vessel to apply pressure on the diaphragm to generate strain on radius direction. In this research, the tensile tester and pressure vessel will be utilized to generate different strain and it will be discussed in the later sections.

To better understand the electrical property of the CNT-PI nanocomposite, the resistance and impedance will be measured. By utilizing electrical impedance spectroscopy, the impedance which includes both real and imaginary part and the capacitance can be obtained. Though the impedance includes the resistance already, a DC current/voltage source measure unit will still be used to test the resistance, because it is more convenient to observe the resistance change with strain at a continuous time domain while impedance spectroscopy capture the impedance at specific times at a frequency domain which roughly covers frequency from zero to infinity.

3.3 NANOCOMPOSITE FABRICATION

There are two major steps to fabricate a thin film piezoresistive sensor: fabrication of the suspension and making the thin film. The quality of the suspension is pretty critical. The mechanical and electrical properties and the piezoresistivity can all be affected, which are majorly caused by the distribution of the carbon nanotube in the composite suspension. Proper procedure of fabrication of suspension makes the carbon nanotubes uniformly distributed in the polyimide and makes it possible to have higher quality of the final nanocomposite. If the carbon nanotubes are not dispersed well in the suspension, it is almost impossible to fabricate the thin film with consistent mechanical and piezoresistive properties, and the data got from the testing may not be reliable and the repeatability won't be good, no matter what kind of method people use to make the thin film of the composite. Once the suspension is fabricated, the thin film shall be made. Since the viscosity of the suspension is relatively small, the liquid is easily moved around on the substrate, inkjet printing technology is utilized to maximize the control of the drops. The amount of suspension on the substrate can be precisely controlled, and so does the distribution of CNT. The thin film is then ready to be heated and the material will be fully cured.

3.3.1 Suspension Fabrication

The carbon nanotube-polyimide Nanocomposite is fabricated by using solution blending method which is the most common method. There are three major steps: disperse nanotube in a suitable solvent, mix with polymer at room temperature and finally cast a film to recover the composite.

N-methyl-2-pyrrolidone (NMP from Sigma-Aldrich®, 1L, St. Louis, Mo, USA) is used as solvent because of its chemical compatibility with both carbon nanotube and polyimide. First, CNT (swCNT commercially available through Aldrich®, 2g, St. Louis, Mo, USA) is dispersed in NMP with a weight ratio of 1:1000, then, magnetic bar is used to stir the suspension at 1200rpm for one hour and ultrasound for three hours using Branson 5200. During this time, polyimide (PI from HD® Microsystem, 1 Gal, Parlin, NJ, USA) is diluted in NMP with weight ratio of 1:2 and stir using magnetic bar at 800rpm for an hour. Suspensions with different CNT concentration are fabricated by mixing the CNT solution and PI solution with different weight ratio. To obtain 1.2wt% of CNT-PI suspension, the ratio of combining CNT suspension and PI solution would be 1201.2:300, similar for 1.4wt% with 1401.4:300, 1.6wt% with 1601.6:300, 1.8wt% with 1801.8:300 and 2wt% with 2002:300. Once they are mixed, stir at 1200rpm for an hour, then put into ultrasonic water bath for around 10 hours and always ultrasonic for two hours every time before print the composite on the substrate.

A thin polyimide film is used as substrate of the deposition of the Nanocomposite. Interdigitated transducer (IDT) electrodes are deposited on the substrate with sputter coater and shadow mask before making the Nanocomposite thin film. Inkjet printing method is used to deposit the nanocomposite on the substrate.

Once it's been print, the thin film should be heated at 120 degree on hotplate for 4 minutes and get it fully curved at 350 degree for one hour in the oven.

3.3.2 Printing Procedure

In order to fabricate a thin film of specific shape by inkjet printer, there are two major steps: generate drops and design the pattern. Based on the principle of inkjet printing technique,

pressure inside the reservoir of the material and the wave form of the voltage applied on the piezoelectric layers in the printer head are the critical parameters need to be controlled to generate uniformly consistent drops. Back pressure of -2.0 kPa is first decided to make sure the pressure is large enough to have drops generated by the voltage and not too large that material would keep dropping from the nozzle without electric voltage applied. If the pressure is too low there won't be material coming out no matter how the wave of the voltage is formed. Then the wave form is decided, and summarized in the following table:

Table 3.1 Voltage Wave Parameter [45]

Action	Time(μs)	Magnitude of Voltage(Volt)
Rise	3	----
Dwell	30	30
Fall	3	---
Echo Dwell	40	-30
Final Rise	1	---

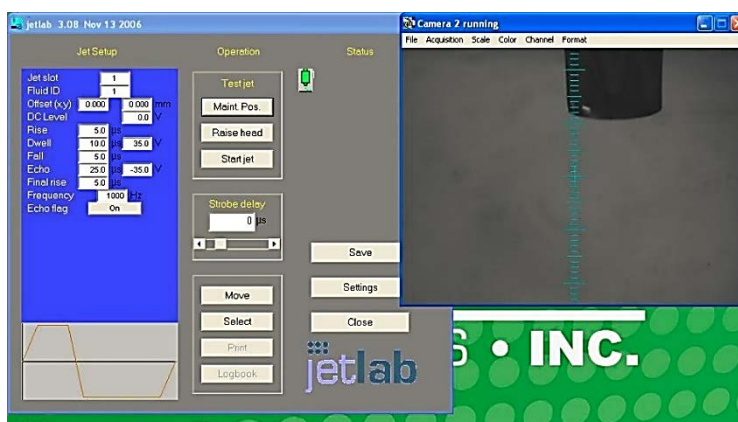


Figure 3.6 Inkjet Printing Station and the operation software [46]

The time and voltage of dwell and echo dwell may vary a little bit depending on the temperature and humidity of the lab environment and the time that material has been fabricated. Once the wave form is set, the size and the velocity of the drop would be pretty consistent even with different carbon nanotube concentration in this case. That is because it is the viscosity of the material to be print that majorly dominant the wave form needed to get good drops and the variety in CNT concentration is too small to affect the viscosity that they share same wave form. Finally, the drops of different CNT concentration are of roughly same size (around 0.1mm in diameter) with different amount of CNT in. That makes it possible to make samples of same or different CNT concentration have same size and pattern.

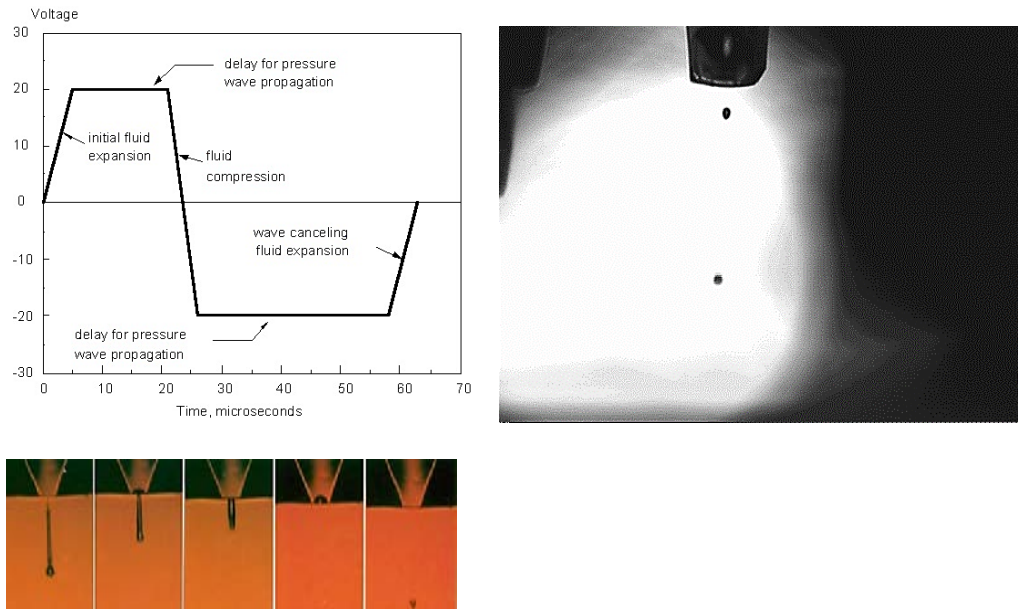
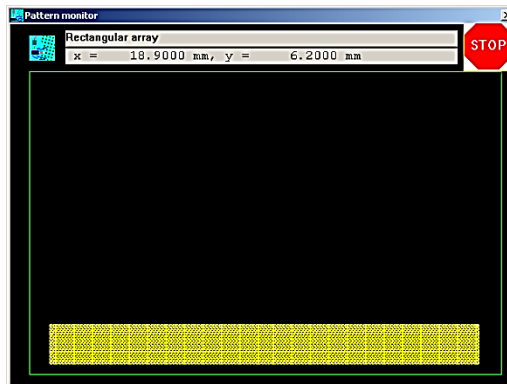


Figure 3.7 Wave form of drop formation, drop generation procedure and the picture of generated drops of CNT-PI suspension [46]

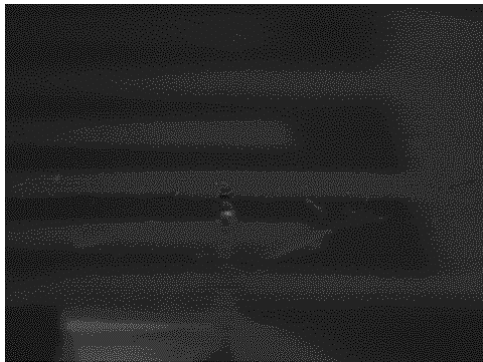
The pattern of printing to have a rectangular thin film is shown in Figure 3.8, the geometry of the pattern is decided by the step size and number of steps on x and y direction. Since the drop sizes are always the same, the step size would be fixed to 0.1mm on both directions and the number of steps would be 160 in x and 13 in y direction. Using the step size that is same with the drop diameter would give continuous rectangle thin film. One layer is build up once the pattern is finished, and it usually cost 30 min to build. In this research, using four layers for each sample to have enough material on the substrate that electric property (piezoresistivity in this case) can be evaluated by the testing method and won't cost too much time to fabricate. The two samples on one substrate for pressure testing are fabricated simultaneously which means after printing the first layer of sample #1, printing the first layer of sample #2 starts and then go back to sample #1 to fabricate the second layer and keep working in this way. So does the samples for tensile testing. In this way, the first layer is almost dried when the second layer is built, it can prevent the flowing around of the suspension when too much

liquid is accumulated, and the later layer would fill the discontinuous spaces between the drops of the previous layer and finally make a continuously uniform thin film.

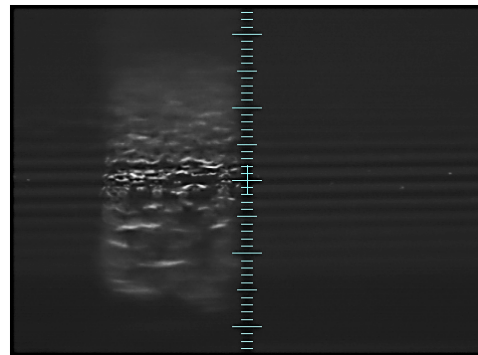
Though tried to use profiler to test the thickness of the thin film, but the substrate is so flexible that it is hard to get the true thickness. So the thickness can only be estimated: given the volume per drop is 120 pL (picoliter 10^{-12} L), making a thin film with $161 \times 14 \times 4$ where print 4 drops per trigger, to get 998400 pL per layer and for a four layer film it is 3.4 mm^3 (3993600 pL), with total area $0.1 \times 160 \times 0.1 \times 13 = 20.8 \text{ mm}^2$, to get thickness $163.46 \mu\text{m}$, and the ratio of CNT-PI to solvent is roughly 1:1000, so the final thickness of the thin film after it curved would be about 163.46 nm .



(a)



(b)



(c)

Figure 3.8 Pattern and Sample printing procedure

Fig 3.8 shows the pattern of the sample (a) and the real time pictures during printing among which (b) shows the first row of drops depositing on the substrate with IDT and the (c) shows the full pattern generated. It shows the precise control of the amount of suspension deposited on the substrate and the geometry of the thin film.

3.4 CNT NANOCOMPOSITE RESPOND TO UNIAXIAL LOAD

To investigate the piezoresistive property, and obtain the gauge factor more specifically, applying a uniaxial load and testing the resistance during the load applies is a direct way. In this section, the uniaxial load will be applied on the substrate. Since the carbon nanotube polyimide thin film has been well curved and attached on the substrate well enough to make the assumption that the load applied on the substrate is equal to the load suffered by the nanocomposite thin film and the longitudinal strain on the substrate is equal to the longitudinal strain of the thin film. Thus, by recording the longitudinal strain on the substrate and measuring the resistance simultaneously, the gauge factors of the nanocomposites with different CNT concentration would be obtained.

3.4.1 Experimental Setup

Figure 3.8 shows a sample that is ready to be tested. The fully curved nanocomposite is generated on a flexible polyimide substrate with interdigitated transducer (acting as electrodes) coated on. The substrate will then be fixed in a stress/strain apparatus (figure 3.9 left, AP8214 from Pasco) which equipped with a force sensor stress calculation and a rotary sensor for

displacement/strain measurement. The ScienceWorkshop® 750 located below the apparatus samples the data and transfers real time data to the computer where a software (Datastudio) would record the data. By rotating the crank of stress strain apparatus clock-wise slowly, a uniaxial load is applied on the substrate. Datastudio start to collect data just when the lever arm contact with the force sensor and it can be stopped whenever there is enough data needed been collected.

In the meantime, the nanocomposite will be connected to a current/voltage source measure unit (figure 3.10 right, Keithley 238) with a Wheatstone bridge building in, and a DC voltage source of 10 volts can also be generated by the measurement unit, so the real time resistance of the thin film can be obtained. A GPIB controller (by National Instrument) is used to transfer the real time data to the computer and recorded by a LabVIEW program.

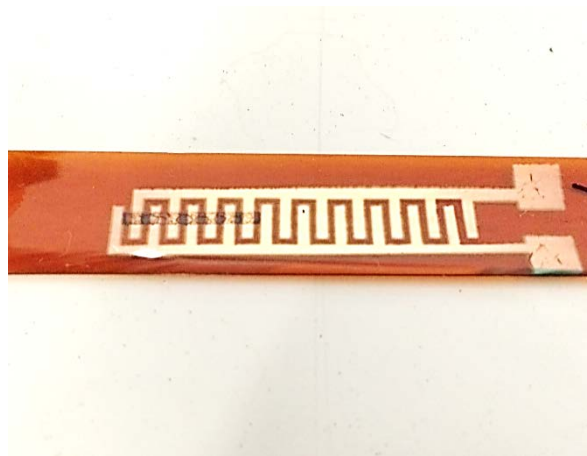


Figure 3.9 Sample photo



Figure 3.10 Testing equipment (stress/strain apparatus (left) and current/voltage source measure unit (right))

3.4.2 Results and Discussions

For the samples with five different carbon nanotube concentrations, from 1.2% to 2.0%, the $\frac{dR}{R}$ vs ϵ (longitudinal strain caused by the load from same direction) can be generated. And the results are shown in Figure 3.11, and the gauge factor can then be summarized in Figure 3.12.

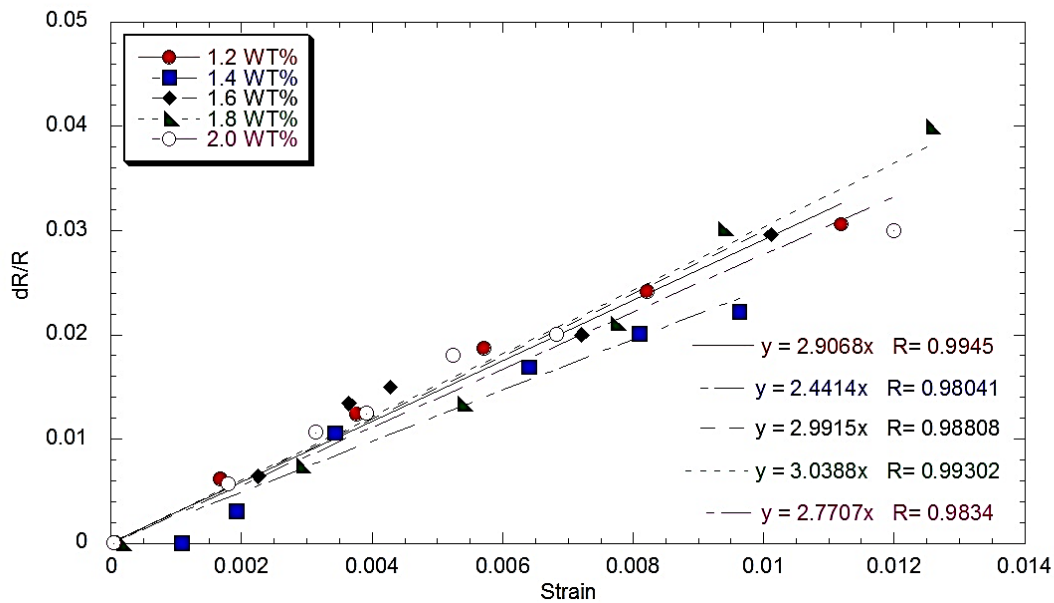


Figure 3.11 Normalized resistances with strain of CNT concentration from 1.2wt% to 2.0%

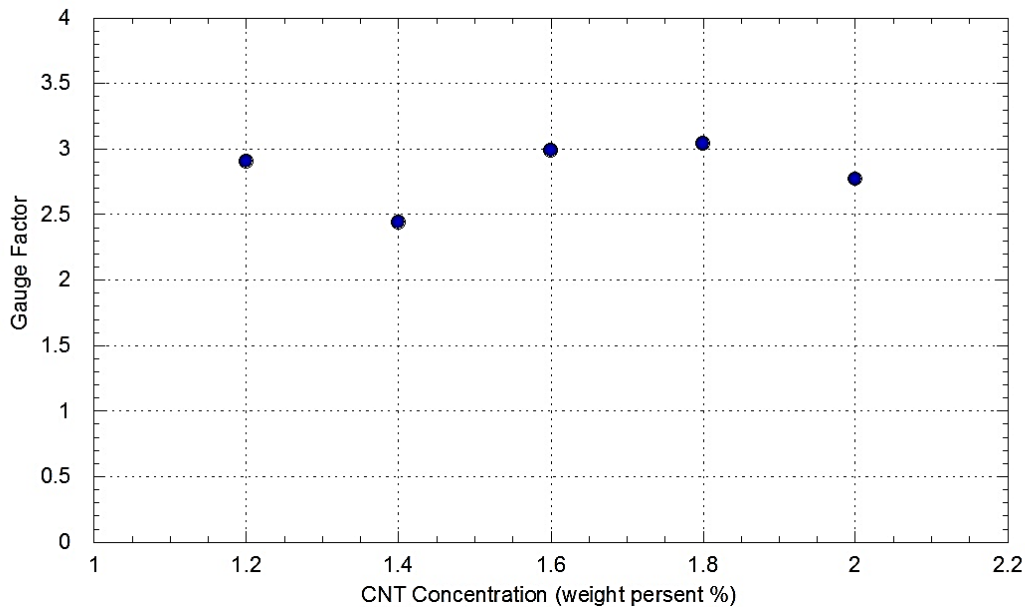


Figure 3.12 Summary of Gauge factor

Based on figure 3.11, it shows that the resistance increase as the extensional load is applied, which agrees with the theoretical prediction based on tunneling effect. And the relationship between resistance changes with strain is approximately linear and this slope is gauge factor which is defined by Equation 3.7. And from figure 3.12, the gauge factors increase as the carbon nanotube concentration increases, considering the fact that the percolation threshold is around 1.5% to 2.0%, and the 1.8% is an optimum choice as strain sensor.

3.5 CNT NANOCOMPOSITE RESPOND TO PRESSURE

The sample for pressure testing is built on circular substrate as shown in figure 3.13, the two thin films on the substrate are two individual thin film with their own electrode pair. They were built simultaneously with same suspension, of the same pattern with same size and heated

together with oven, and they would be testing together with same pressure at same time. They are also mirror image of each other through the line which go through the center of the circular substrate and parallel to the electrode ‘fingers’. By testing the impedance of the two samples, not only the electrical property of the nanocomposite can be investigated, but the repeatability of the fabrication method of the inkjet printing will also be examined.

The diameter of the substrate is 10 mm, while the effective part would be a concentric circular area of 6 mm in diameter which is also the dimension of the pressure vessel. Each thin film is a rectangle of 13 mm by 1.3 mm, so when pressure is applied, the strain on radial direction of the substrate can be taken as the same as the strain on the longitudinal direction of the thin film.

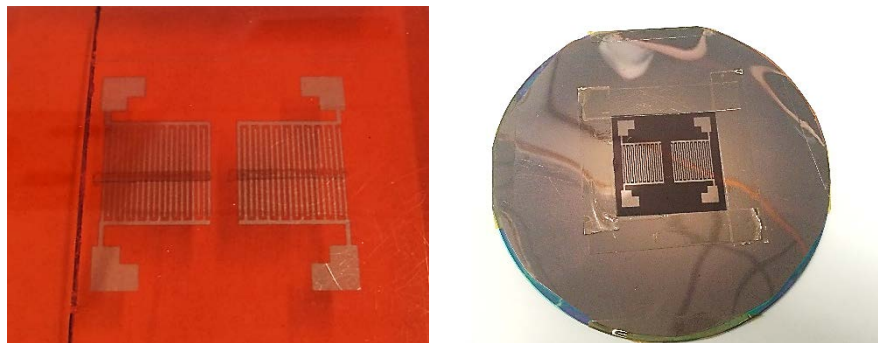


Figure 3.13 Sample photo

3.5.1 Experimental Setup

A pressure vessel (shock tube) is used to test the piezoresistive property of the nanocomposite with pressure. The nanocomposite is fixed and sealed in the pressure vessel, and the pressure comes from the back of the substrate which means the thin film will be suffering extension. The main objective is still to calibrate the gauge factor of the nanocomposite. But apart from that, using the set up shown in figure 3.14, the at each pressure state, the deformation

of the substrate is stationary which gives stationary strain, it is possible to precisely identify the resolution for the nanocomposite working as strain/pressure sensor. And it can also reversely, make the samples working as pressure sensor after the gauge factor is calibrated.

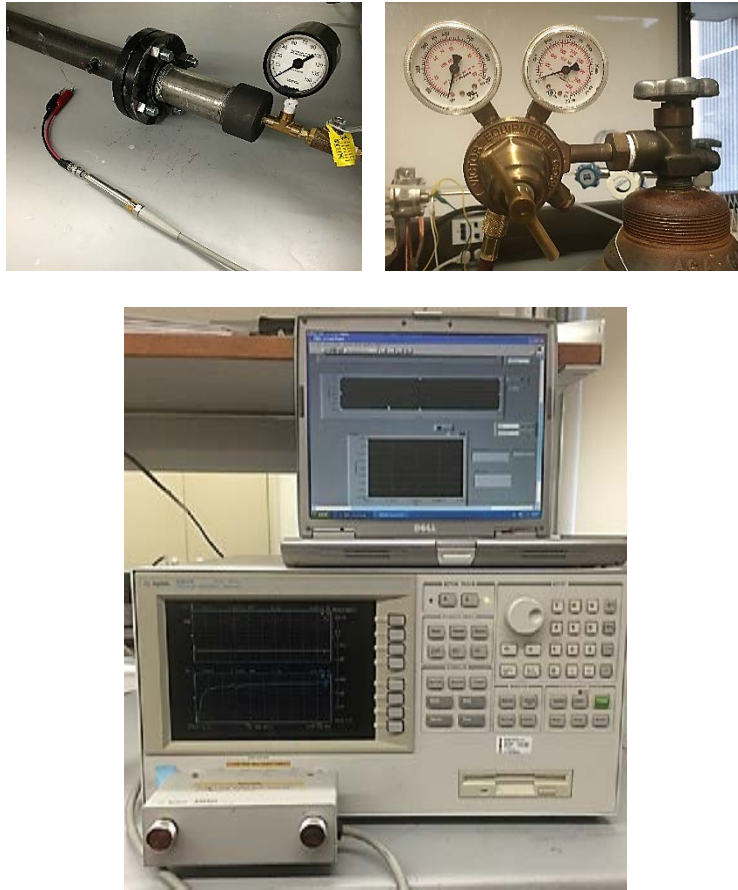


Figure 3.14 Testing Equipment

The pressure vessel is connected to a pressure regulator and then to a compressed gas tank working as the pressure source. By changing the pressure, there is strain on the substrate and so does the nanocomposite thin film. The pressure can be read from the regulator and the nanocomposite is connected to a precise electrical impedance analyzer (Agilent 4294A). Electrical impedance spectroscopy can measure the impedance of a device by applying a small AC current excitation signal and measuring the voltage drop across the device over a range of frequencies, and that will produce the frequency spectra of resistive and reactive components of

the equivalent electrical impedance of the device. So the Cole-Cole plot can be made based on the data collected. The impedance analyzer can sweep a frequency from 40 Hz to 110 MHz, which makes a full semi-circle in a Cole-Cole plot. Based on the plot, the maximum $\text{Re}(Z)$ ($\text{Re}(Z)$ at the lowest frequency) represents the summation of the series resistance and the parallel resistance to the capacitance. And the minimum $\text{Re}(Z)$ ($\text{Re}(Z)$ at the highest frequency) represents the series resistance can usually be taken as negligible. The maximum $-\text{Im}(Z)$ of the semi-circle, C is the equivalent capacitance and τ is the time constant of the material.

3.5.2 Results and Discussions

The pressure testing results of the nanocomposite with CNT concentration of 1.2%, 1.4%, 1.6%, 1.8% and 2.0% are shown in figure 3.15 to 3.19. They show how impedance changes with the change of pressure.

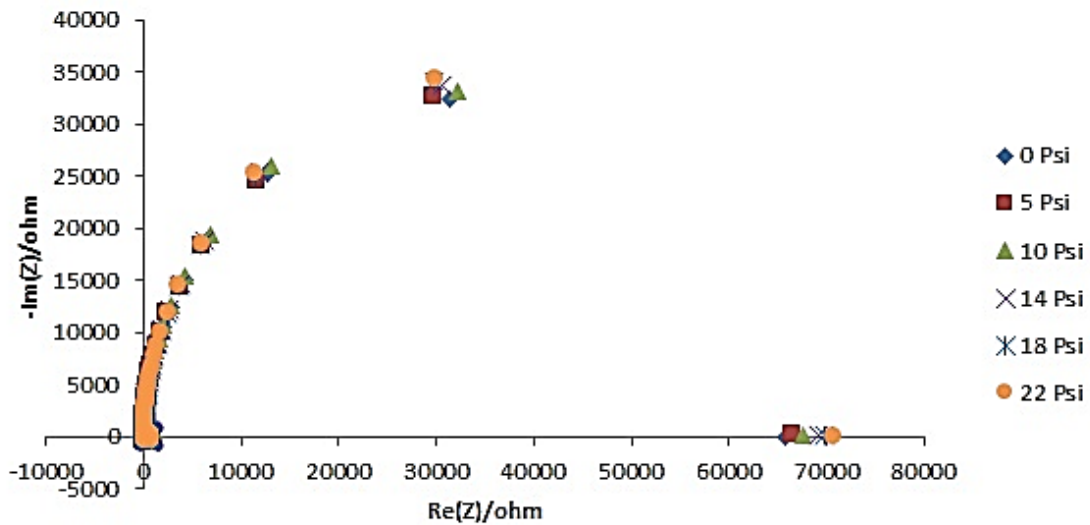


Figure 3.15 Impedance of test sample with CNT concentration of 1.2wt%

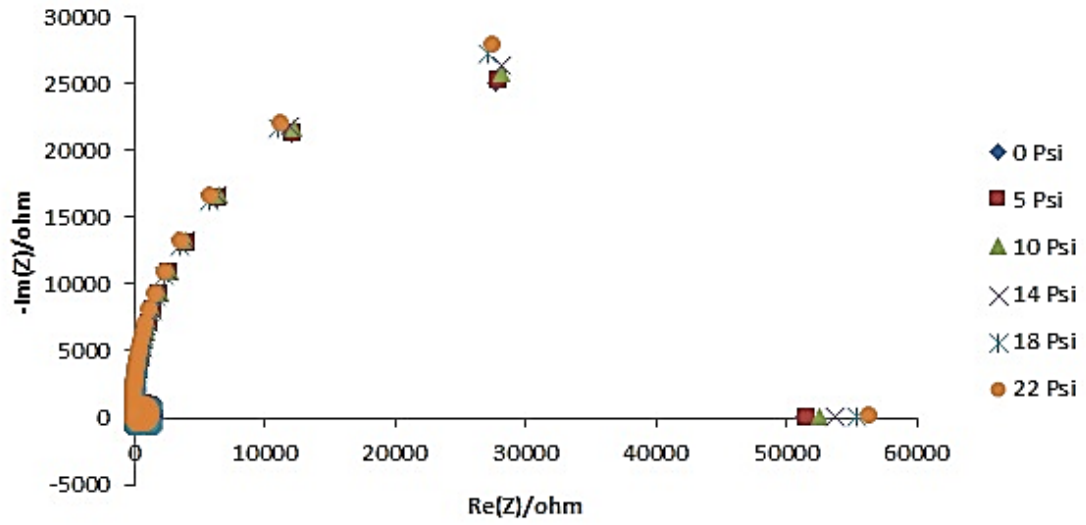


Figure 3.16 Impedance of test sample with CNT concentration of 1.4wt%

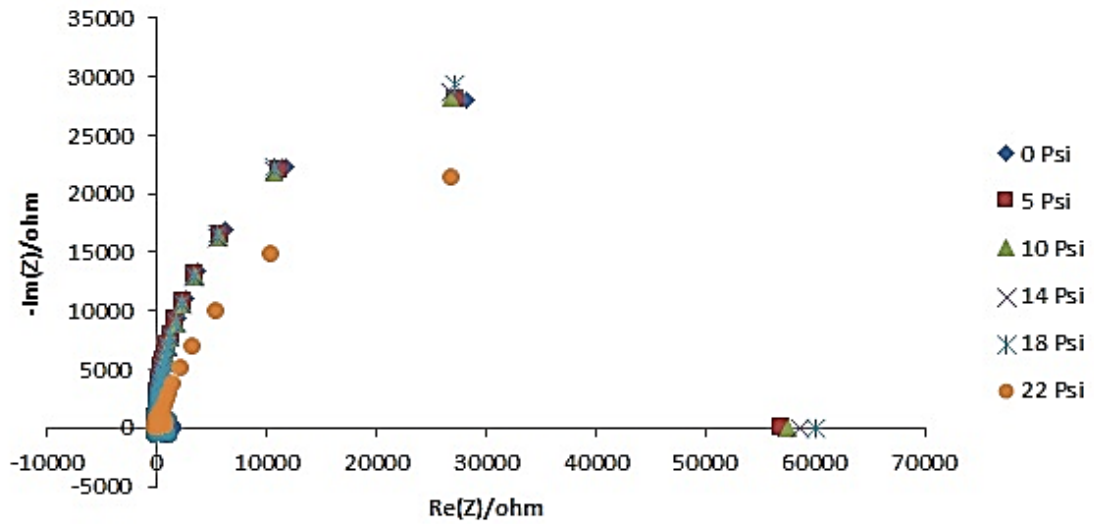


Figure 3.17 Impedance of test sample with CNT concentration of 1.6wt%

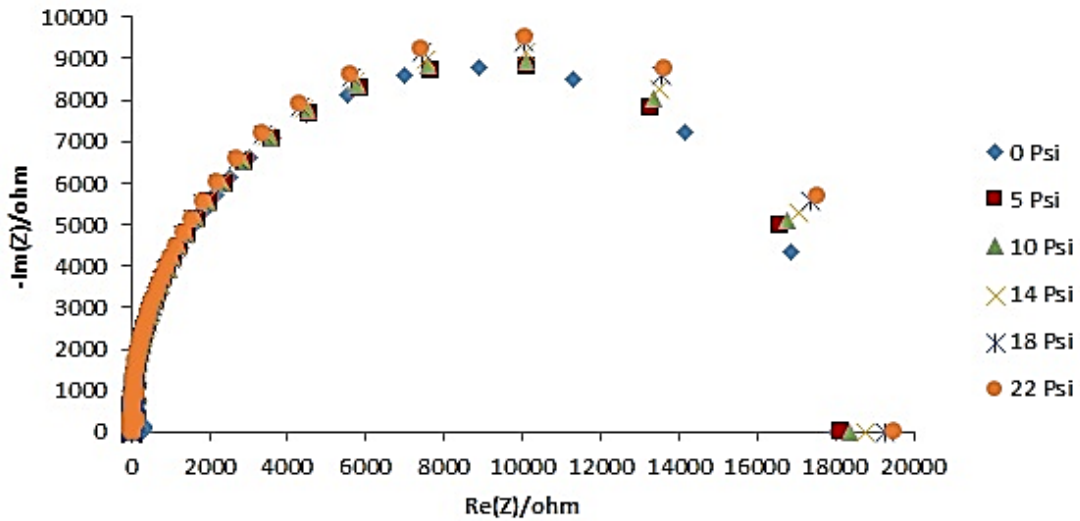


Figure 3.18 Impedance of test sample with CNT concentration of 1.8wt%

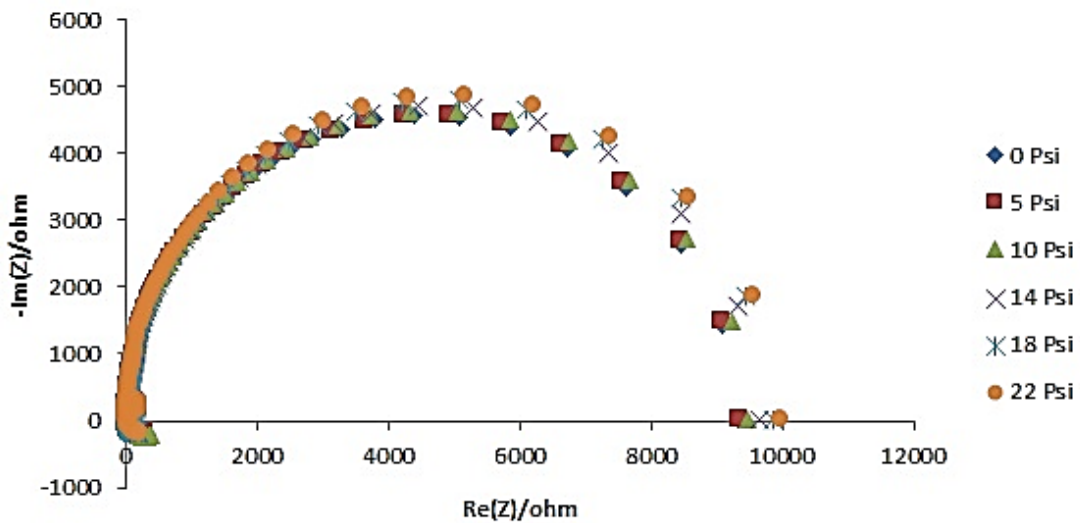


Figure 3.19 Impedance of test sample with CNT concentration of 2.0wt%

Based on the Barlow's equation, the stress on the substrate can be calculated based on the pressure applied and the geometrical information of the substrate. And based on the linearized Hook's law, the strain can be calculated. Since the assumption has been made that the strain on

the substrate is equal to the strain on the thin film, the relationship of resistance change with strain can be estimated and the gauge factor can be obtained.

The strain correspond to each pressure level is shown in Table 3.2

Table 3.2 Strain on substrate corresponding to Pressure

P (Psi)	Stress (Psi)	Strain
0	0	0
5	1500	0.004137
10	3000	0.008274
14	4200	0.011583
18	5400	0.014892
22	6600	0.018202

So the resistance change with strain can be plotted and the gauge factors are summarized.

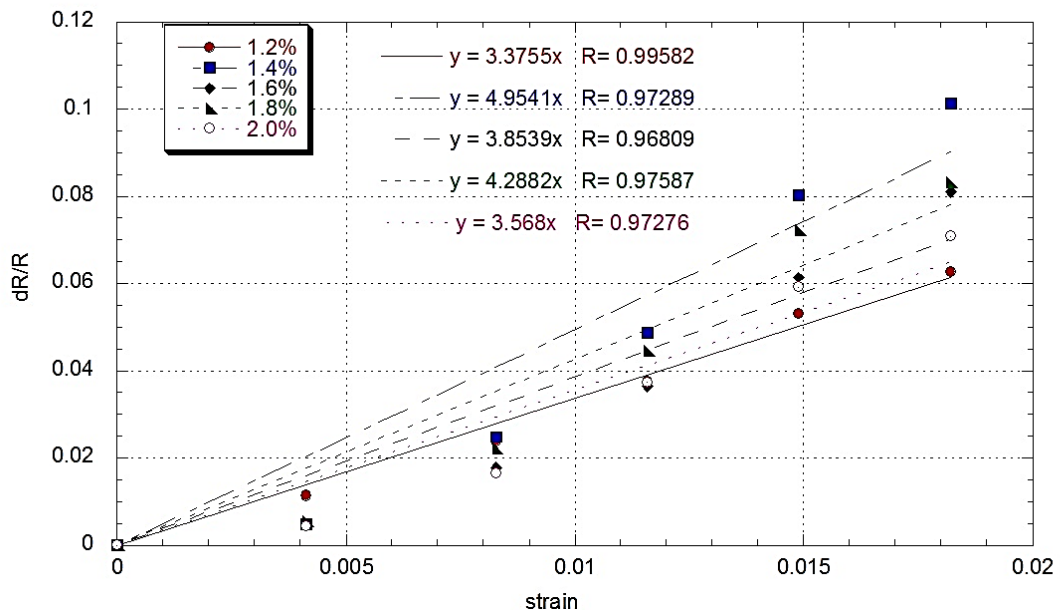


Figure 3.20 Resistance change with strain of the five nanocomposites

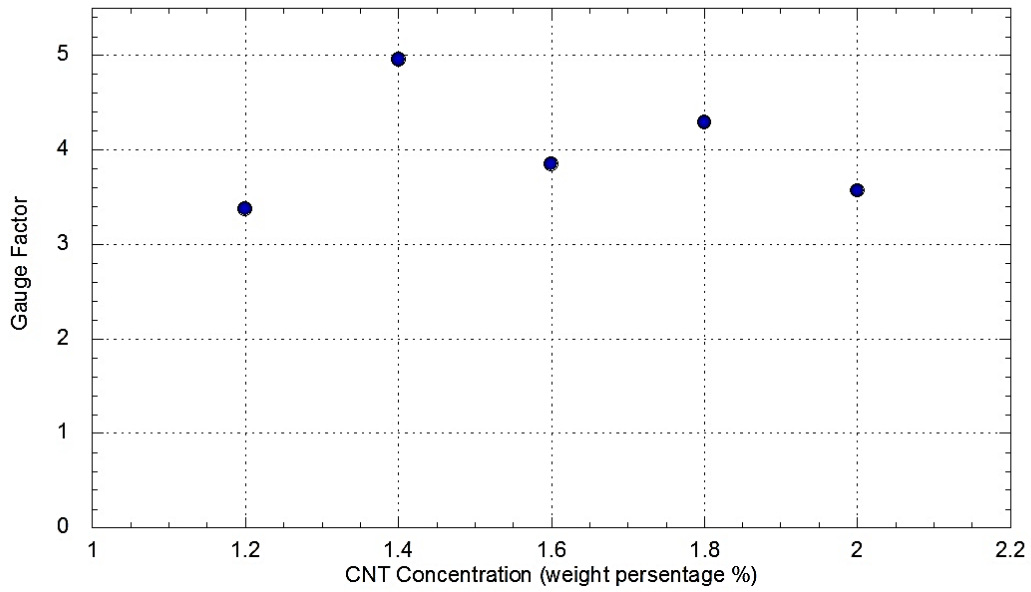


Figure 3.21 Gauge factor/sensitivity of resistance summary

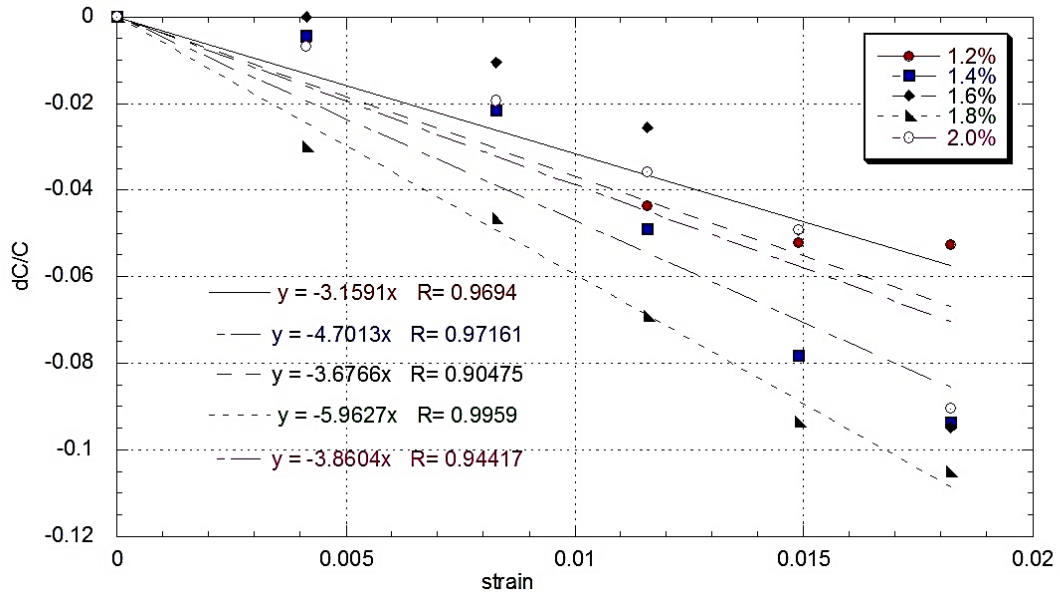


Figure 3.22 Capacitance change with strain of the five nanocomposites

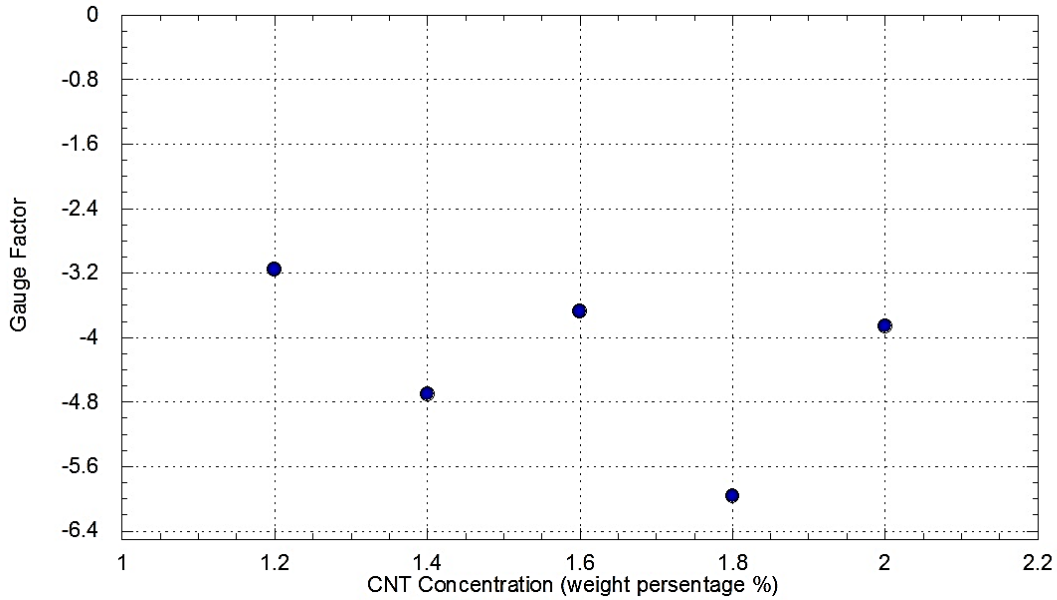


Figure 3.23 Gauge factor/Sensitivity of Capacitance summary

Based on figure 3.20, it shows that the resistance increase as the extensional pressure is applied, which agrees with the theoretical prediction based on tunneling effect. And the relationship between resistance changes with strain is approximately linear and this slope is gauge factor which is defined by Equation 3.7. And from figure 3.21, the increase in gauge factor slows down beyond carbon nanotube concentration of 1.4%, and varies slightly around 5. Comparing with the gauge factors from tensile testing, choosing 1.8% nanocomposite should still be a good choice.

Figure 3.22 shows the capacitance change with strain. The capacitance decreases as the pressure is applied and it can be estimated as a linear relationship between the normalized capacitance and strain. Since the equation of parallel plate capacitance is

$$C = \epsilon_r \epsilon_0 \frac{A}{d} \quad (3.11)$$

Where ϵ_r is the dielectric constant, ϵ_0 is the electric constant, A is the cross section area of the strain sensor and d is the distance between the electrodes.

Under extensional force, there would be a decrease in cross section area and an increase in distance which finally cause the decrease in capacitance. Figure 3.23 indicates that the magnitude of capacitance also increases as the concentration of carbon nanotube grow. The growth also slow down after concentration go beyond 1.4% and vary around 5, which means the 1.8% nanocomposite is also a good choice as sensor testing capacitance under strain. The absolute value of gauge factor of resistance and capacitance are quite similar so the sensitivities of the measurement of both are also similar.

3.6 CONCLUSION

3.6.1 Printing technique

From Figure 3.15 to 3.19, the semi-circles are not quite complete, especially for samples with lower CNT concentration, which may be caused by agglomeration of the material during the printing procedure. This lower amount of CNT in the composite is reasonable, because the agglomeration would have a more serious impact on the electric and piezoresistive properties. So an improvement is made when fabricating the samples for temperature by changing the materials in the reservoir during printing.

3.6.2 Tensile testing and Pressure testing results comparing

By comparing the gauge factor obtained by tensile testing and pressure vessel testing, the change in gauge factor with respect to strain obey the similar trend which is the increased slowing as concentration of carbon nanotube go beyond 1.4% and varying slightly around certain value. However, the gauge factors from tensile testing are all smaller than those from pressure testing.

There are factors that may challenge the credibility of the result of tensile testing. When the sample is being tested on the instrument, there is always torsion on the sample, and when the sample is twisted, the actual deformation of the thin film would be different from the deformation caused by pure uniaxial strain. That may make the resistance changes of the thin film different from the changes under uniaxial tension. The other factor is that the resistance and the strain were collected by two programs; one collected data every 0.1 second while the other every 1 second. There were always misalignments, because the results were collected based on different timelines.

The results from pressure testing eliminate the effects. By fixing the boundary of the sample, the pressure would only vary on the radius direction, which makes no torsion on the sample. It makes it possible to keep the substrate deformation at some specific strain so that the impedance can be collected at a relatively steady state. However, the data of the pressure testing may also have flaws. Although, the ratio of the two edges of the rectangular thin film is high, the deformation of the thin film is not uniform on the short edge which along radius direction of the circular substrate. The simplified Hook's Law does not precisely describe the stress strain relationship. Modifications on the gauge factor definition and the shape of the transducer will be discussed in the following chapters.

Regardless of the possible errors on the value of gauge factors from the testing methods, the trend of the variation of the gauge factors from the both methods are still similar, so the optimum choice of the nanocomposite can still be made.

4.0 CNT-POLYIMIDE NANOCOMPOSITES RESPONSE TO TEMPERATURE

4.1 INTRODUCTION

Most strain sensors would work in environments with variation in temperature, while temperature fluctuation would cause the change in size of the strain gauge, so that the resistance of the sensor would change. The variation in resistance would be taken as strain if the effect has not been compensated and that would cause error in the usage of the sensor. So it is very important to study the relationship between the changes of resistance of the CNT-Polyimide nanocomposites and temperature variation, and then compensate the effect when designing the sensor.

In this chapter, the theoretical relationship between the temperature and resistance changes will be first described, and then experiments would be conducted to measure this relationship and get the temperature coefficient factor. Finally, a compensation method would be described.

4.2 TEMPERATURE COEFFICIENT FACTOR

Since it has been proven that piezoresistive materials are much more sensitive to environment (especially the temperature variation) than metallic strain gauges, it is necessary to study the

relationship between the resistances changes with the temperature. The resistance-temperature relationship is usually approximated by the following linear expression [1]:

$$R = R_0[1 + \alpha(T - T_0)] \quad (4.1)$$

Where T_0 and R_0 are reference temperature and the resistance at reference temperature respectively, and α is the temperature coefficient of the material that is to be determined by experiment.

4.3 EXPERIMENT

4.3.1 Testing Setup and Procedure

When fabricating the samples, the same procedure of making suspension and printing are used with the samples for pressure testing in chapter 3, apart from only one difference: changing the ‘ink’ during printing. To ‘change ink’, remove all the material left in the reservoir and replace it with the suspension that has been ultrasonic in the water bath during the printing period. Since two samples will be made simultaneously, the printing time for each layer would be 30 min. After the first layer of the sample#1 is made, fabrication of the first layer of sampler#2 starts, so, if change the material in the reservoir every one hour and a half, the final two samples with four layers in total should have same quality of materials. Also, by changing the material, the distribution of the CNT in the suspension would be better than the suspension stays steady in the reservoir for six to eight hours when agglomeration of CNT could occur.

In order to evaluate the response of the resistivity of the transducer with temperature changes, the transducers of different carbon nanotube weight ratio is heated on the hotplate

simultaneously. Since the transducers themselves are so thin that we can assume the temperature the transducer is suffering is identical the same with the temperature on the hotplate. The room temperature of the lab is 20°C which is chosen as the starting point of the experiment, and it would be taken as the reference temperature, then increase to 50°C, and following up with a 25°C increasing step size of the temperature to finally get the temperature coefficient of the nanocomposites. After each temperature increase, testing on the impedance would be conducted. The results from testing are shown in the next section and discussion on the results will be conducted afterwards.



Figure 4.1 Hotplate for temperature control

4.3.2 Testing Results

The impedances of the samples from 1.2% to 2.0% were tested, and the results are shown in Fig. 4.3.2 to 4.3.6.

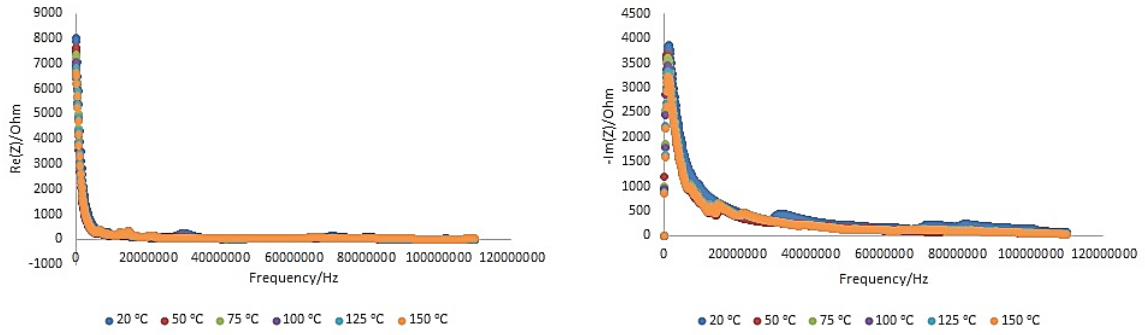


Figure 4.2 Impedance of test sample with CNT concentration of 2.0 wt% with respect to frequency

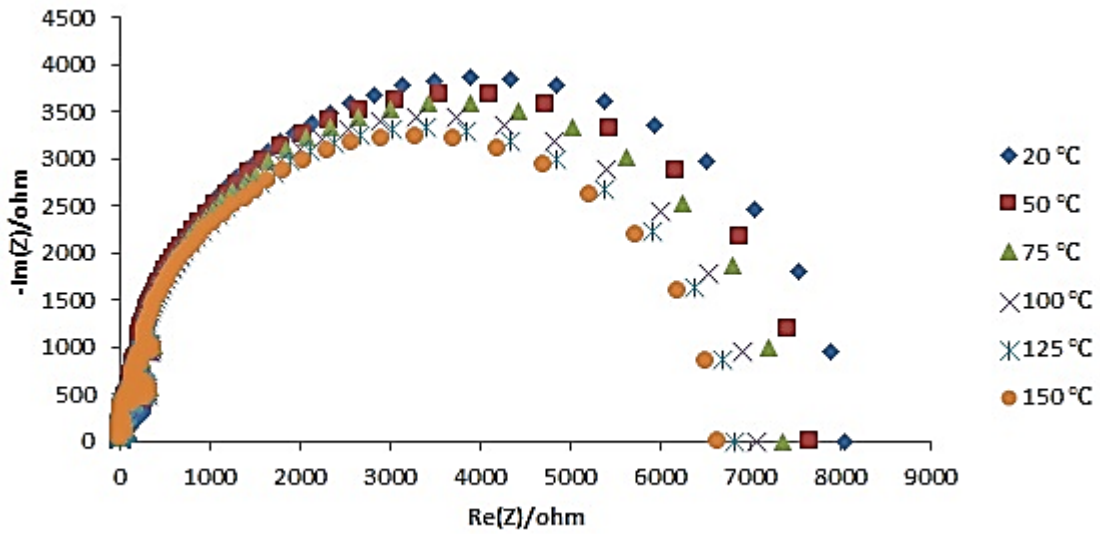


Figure 4.3 Impedance of test sample with CNT concentration of 2.0wt%

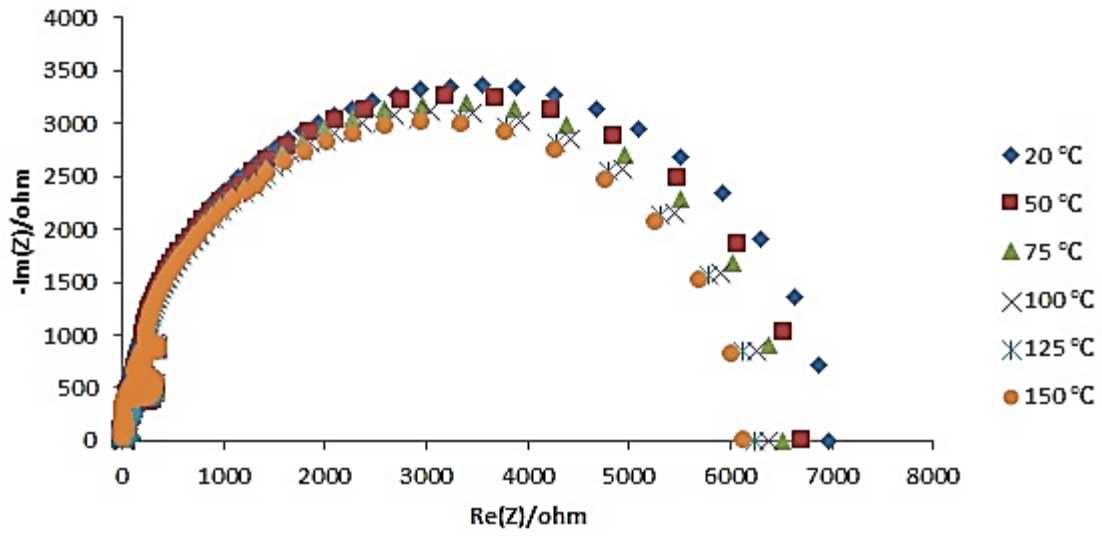


Figure 4.4 Impedance of test sample with CNT concentration of 1.8wt%

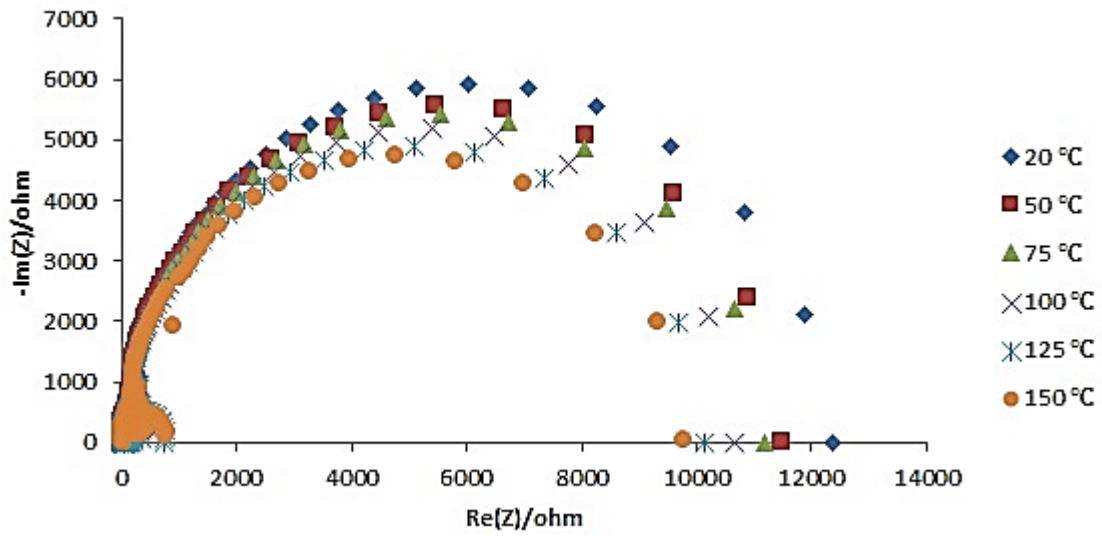


Figure 4.5 Impedance of test sample with CNT concentration of 1.6wt%

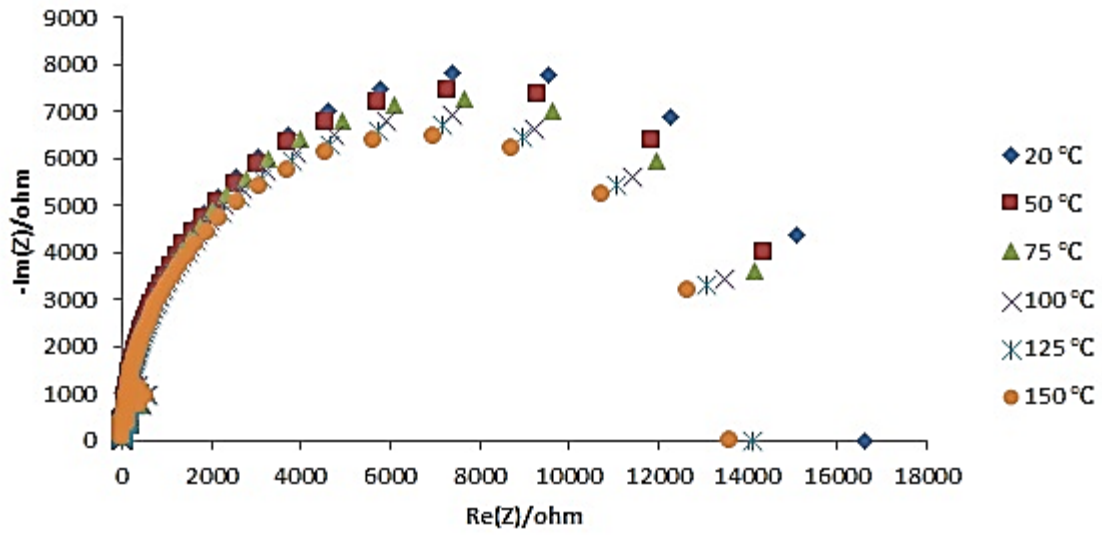


Figure 4.6 Impedance of test sample with CNT concentration of 1.4wt%

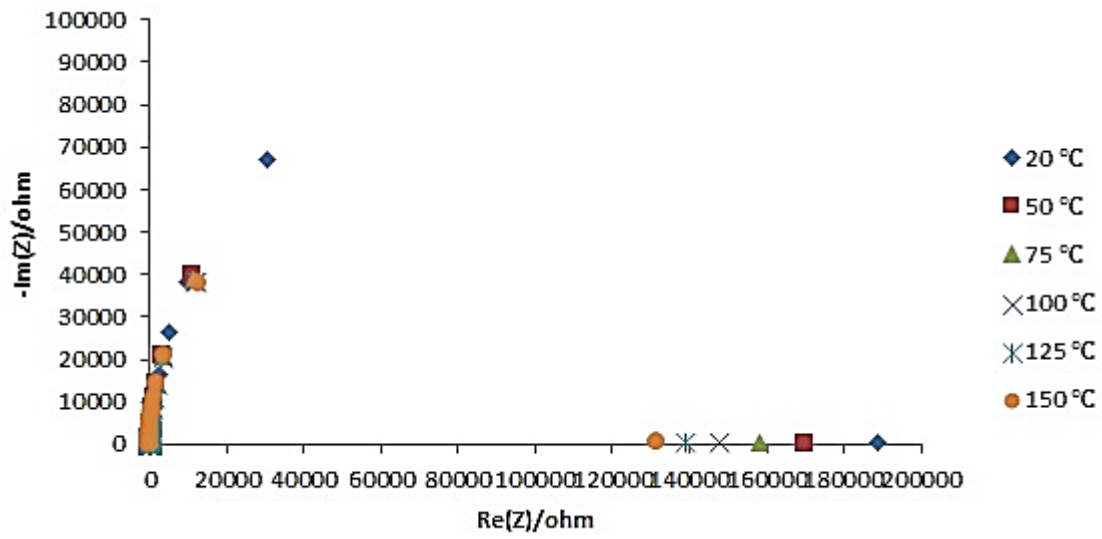


Figure 4.7 Impedance of test sample with CNT concentration of 1.2wt%

4.3.3 Discussion and Conclusions

Depending on the semi-circles shown in figure 4.3 to 4.7, the impedance of the samples at low frequency (40 Hz) can be extracted. It is a real value, and it is the DC resistance of the sample. The resistances' changes with temperature are plotted in Figure 4.8 and the temperature coefficients are plotted in Figure 4.9.

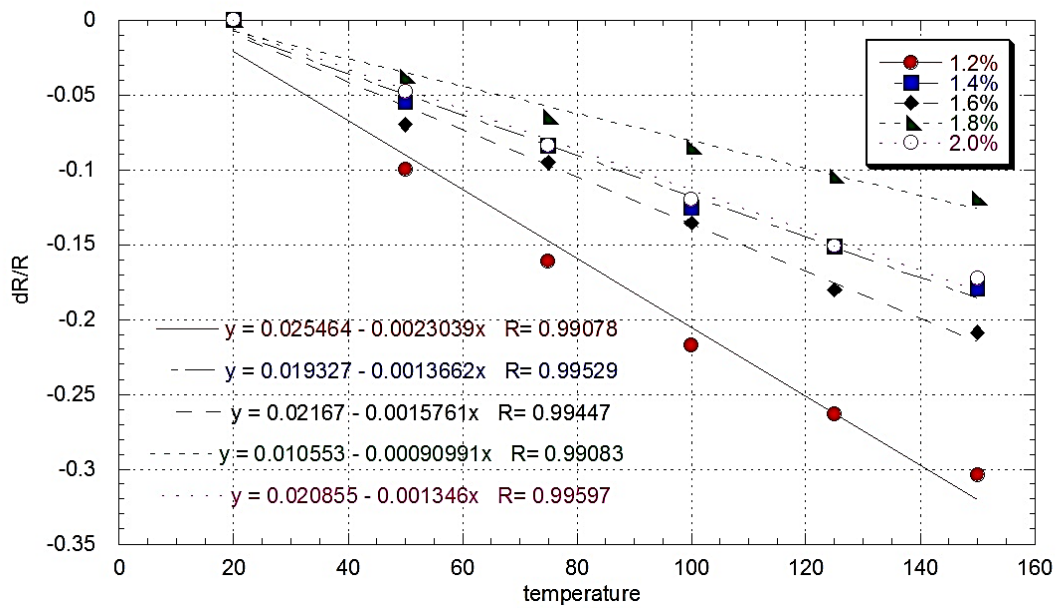


Figure 4.8 Resistance change with temperature of CNT nanocomposites with different CNT concentration

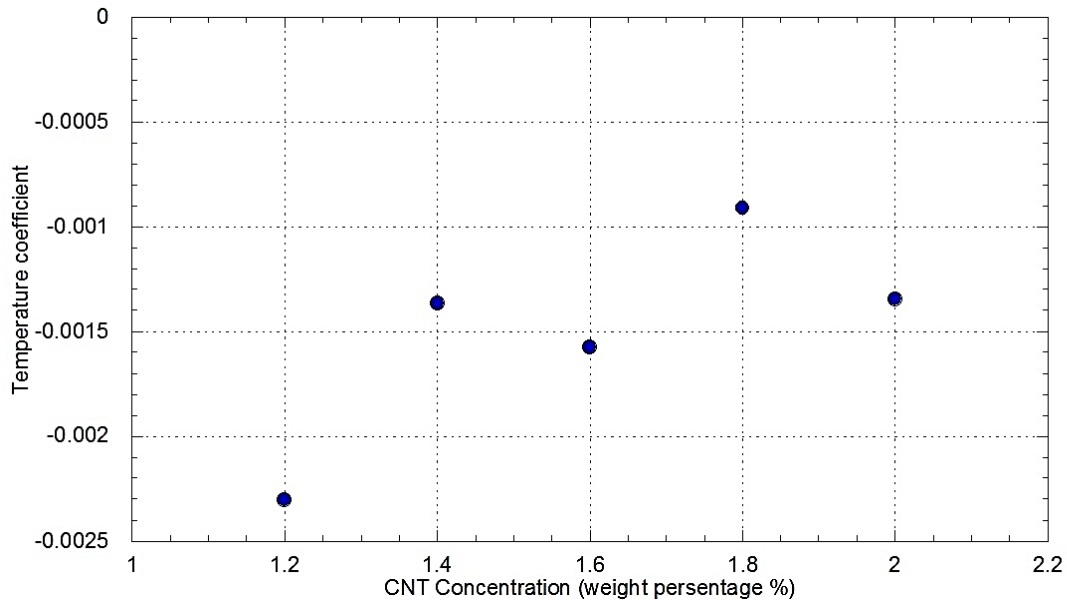


Figure 4.9 Normalized Temperature Coefficient for CNT nanocomposites with different CNT concentration

From figure 4.3-4.7, there is quite an improvement in the completeness of the semi-circle of lower CNT concentration. It confirms that the incompleteness in the semi-circle of samples for pressure testing is caused by CNT agglomeration, and the changing of ‘ink’ is an efficient way to eliminate this effect. The improvement in the suspension procedure like doing functionalization of carbon nanotube before making the carbon nanotube suspension and utilizing higher power of ultrasonication may also give better results, but these won’t be discussed in this research.

Based on Figure 4.8, the resistance decreases as the temperature increases, and the relationship between the resistance changes with temperature follows linear relationship. So if the temperature effect is not properly compensated, when the working environment has a higher temperature than the calibration environment, the resistance change with strain would be underestimated and if working environment has the lower temperature, it would be overestimated. Either way will make the error in application of the transducers in strain/pressure testing. These

results also imply how important it is to consider the temperature effect on the performance of the semiconductor piezoresistive sensor (CNT-polyimide nanocomposite piezoresistive sensor in this case).

From both figure 4.8 and 4.9, it is shown that the temperature coefficient increases as the concentration of CNT increases, which implies that transducer of higher concentration of CNT will be less sensitive to the temperature and the resistance change caused by temperature change is less severe than the ones of lower CNT concentration.

It is also proved in the testing procedure that the impedance change immediately when the actual temperature on the hotplate approaches the targeting value, and in 1 second, the impedance would be steady and remains unchanged until the temperature change again. Also, as long as the temperature changes between 20 °C and 150 °C, the thermo-expansion of the transducer is 'elastic', which means the resistance will always change back to the original value once the temperature drops back.

By using the temperature coefficient, it is possible to compensate the temperature effect on the transducer. There are several ways to compensate the temperature effect. Dummy gauge is one of them. A dummy gauge should have same temperature coefficient with the active gauge, they can be devices with same material same geometry. A dummy gauge is placed next to the active gauge suffering same environment and should not be subjected to any strain. The dummy gauge is then connected to the Wheatstone bridge to the testing the active gauge to cancel out the temperature effect.

Table 4.1 Temperature Coefficient Summary

CNT concentration	Reference resistance (ohm)	Normalized temperature coefficient
1.2%	188848.1	-0.0023
1.4%	16603.74	-0.0012
1.6%	12348.44	-0.0016
1.8%	6970.561	-0.0009
2.0%	8033.886	-0.0013

5.0 CNT-POLYIMIDE NANOCOMPOSITES RESPONSE TO HUMIDITY

5.1 INTRODUCTION

Apart from temperature, humidity is another factor that would affect the performance of the nanocomposite strain sensor. How the humidity affects the electric property of the nanocomposite should be studied. Theoretically, it should be the gauge factor change with humidity of the nanocomposites should be evaluated, but due to the fact that neither the tensile testing nor the pressure testing system is suitable working in harsh environment which humidity change dramatically, here, the DC resistance change with humidity would be measured instead. If resistance does change with humidity, to prevent the humidity effect on gauge factor, actions to prevent the humidity effect should be conducted. Since Parylene has been proven to be a good moisture barrier, parylene will be coated on the thin film if needed.

5.2 EXPERIMENT

5.2.1 Testing Setup and Procedure

There are several methods to control the humidity of the environment. There are commercialized humidity testing systems with high accuracy humidity manipulation, and there is saturated salt

solution method to make several fixed humidity level in an enclosed chamber. But, here since the samples are small and flexible, another method will be used. Figure 5.1 shows the setup for humidity control. The chamber used here is so small that about 1000ml of water could affect the humidity inside the chamber dramatically. So, after put the samples of different CNT concentration on the stage, a container with 1000 ml warm water of 60 °C would be placed beneath the samples. A thermometer and a hygrometer are then placed in the chamber. After about one hour, the humidity stays at the relative humidity of 97% and the temperature inside the chamber stays around the room temperature which is 20°C. That is when the water is replaced by a container with 5 grams of dry P₂O₅ which is a strong desiccant. After the replacement, the humidity in the chamber is about 95%, and then it will gradually decrease. The resistances of the samples are then measured by a multi-meter at humidity from 90% to 10% with the humidity step size 10%. The testing results are then normalized and the resistances at 30RH% are taken as the reference because it is the room humidity in the lab.



Figure 5.1 Chamber Setup

The testing results shows a change in resistance with humidity for all the samples measured, so it is necessary to build a barrier to block the water vapor. In this experiment, 0.5 grams of Parylene powder is used, and the coating is conducted by using Specialty Coating

System PDS 2010. A 250 nm thick layer of parylene is generated covering the surface of nanocomposite thin film. Then the humidity testing procedure is conducted again.

5.2.2 Testing Results

The normalized resistance with humidity change of the nanocomposite of concentration of 1.2wt%, 1.4wt%, 1.6wt%, 1.8wt% and 2.0% are plotted in figure 5.2, where the resistance at relative humidity of 30% is taken as the reference resistance. And in figure 5.3, the resistance change with humidity is shown after the samples were coated with parylene.

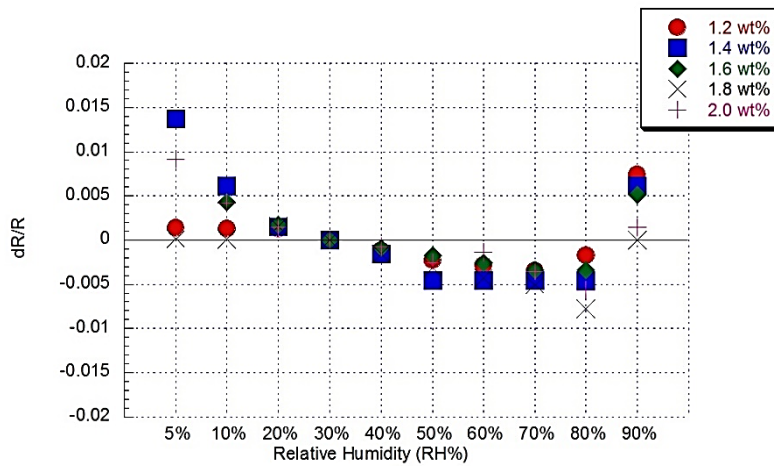


Figure 5.2 Normalized Resistances response to Humidity

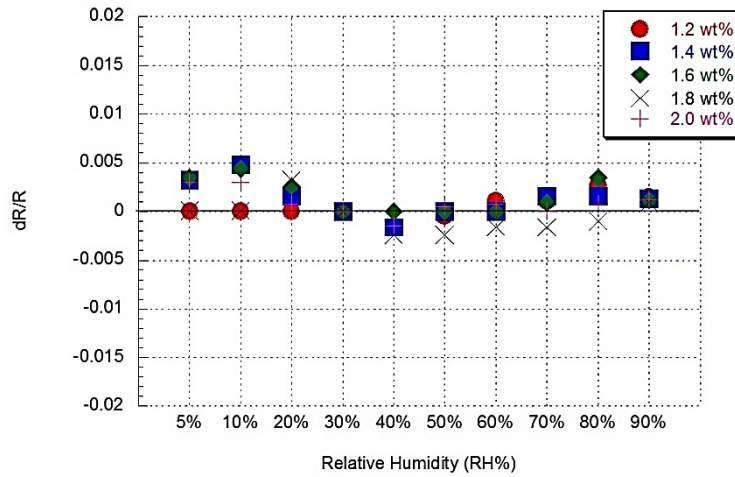


Figure 5.3 Normalized Resistance response to Humidity with Parylene Coating

5.2.3 Discussion and Conclusions

The DC resistances of the nanocomposites do change as humidity in the environment varies. Figure 5.3 shows that regardless of the difference in CNT concentration, all the nanocomposites have the change in resistance with humidity following similar trend. At humidity below 30%RH, as humidity decrease, the resistances increase and the change can be as high as 0.015. While, when the humidity increase from 30%RH to 80%RH, the resistance decrease as humidity increase, until humidity rise to 90%RH, that all the samples have a rise in resistance. Apart from at humidity at 90%RH, the resistance change of the nanocomposite with different carbon nanotube concentration are very similar, showing as a lot of overlap in figure 5.3. This means among the concentrations chosen in this research, the nanocomposite have similar property respond to humidity.

After the parylene coating, the changes in resistance drop to almost zero at humidity from 20%RH to 80%RH. Even for 10%RH and 90%RH, though not zero, the resistance change drops to at least 1/10 of ones before parylene coating. This means, parylene packaging does eliminate the humidity impact on the electric property of the nanocomposite.

6.0 GEOMETRY EFFECT

In the previous chapters, the gauge factor or sensitivity was calibrated by fabricating sample of rectangular shape with length ten times larger than its width. For uniaxial tension, transducer with this rectangular shape should have relative precise gauge factor. But, in practice, the sample or transducer suffer from biaxial deformation under uniaxial tension, and rectangular shape can't fully reflect the deformation under pressure. In this chapter, the mathematical descriptions of the resistance of trapezoid and ring are derived and the sensitivity is then defined. Thanks to the advantages of inkjet printer, it is possible to build trapezoidal and circular pattern. Experiments are then conducted to get the sensitivity of CNT-PI nanocomposites with 1.8wt% of CNT with trapezoidal and circular shape with uniaxial load or pressure.

6.1 SUSPENSION FABRICATION (1.8%WT CNT)

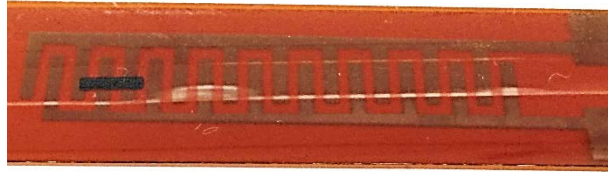
CNT is dispersed in to NMP with weight ratio of 1:1000, and PI is diluted in to NMP with weight ratio of 1:2. These two suspensions are then stirred at 1200 rpm for 3 hours separately and the CNT suspension is put into ultrasonic water bath for 5 hours. Then these two suspensions were mixed together, and stir for another hour. Then this suspension would be ultrasonic for 10 hours till it is ready to be printed.

Table 6.1 Suspension Fabrication

1.8WT%	CNT	NMP(CNT)	PI	NMP(PI)
Nominal	0.018g	18g	0.982g	1.964g
Actual	0.0181	18.0346	1.0566	2.1190
			Use 2.9338(2.946g)g total	

6.2 PRINTING PROCEDURE

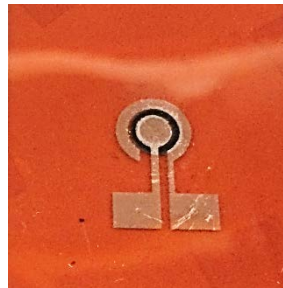
In order to make continuous pattern by drop-on-demand inkjet printing technique which generate discrete drops, the step size of the movement of printer head is set to be smaller than the diameter of the drops, so there would be overlap of the drops. This overlap is necessary to build continuous pattern but may affect the distribution of the CNT on the substrate because the large percentage of NMP make the suspension with low viscosity and the CNT would flow around caused by the interaction of the drops. To eliminate this interaction, a rubber heater is placed on the stage of the printer; it can heat up the substrate to 120 °C to speed up the evaporation of NMP. Observation through the experimental procedure shows the NMP in one drop can be totally evaporated before next drop is placed, so the interaction between the drops is eliminated. The photos of the samples are shown below:



(a) Rectangle



(b) Trapezoid



(c) Ring

Figure 6.1 Photos of Sample

The samples of rectangle and trapezoid shape were put into tensile tester to calibrate the gauge factor. The pressure vessel was used for the measurement of ring shaped, and the center of the ring was the same with the round substrate.

6.3 FORMULA DERIVATION

6.3.1 Trapezoid

6.3.1.1 Definition for resistance

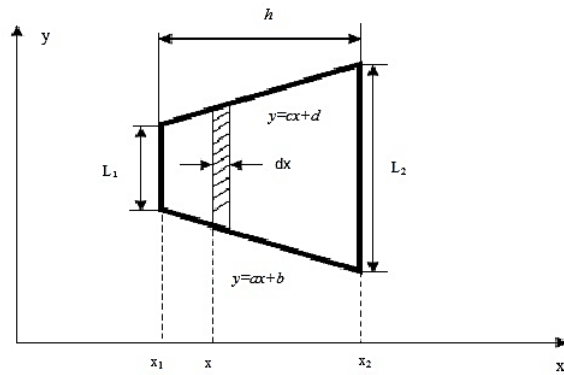


Figure 6.2 Trapezoid

$$dR = \rho \frac{dx}{[(c-a)x+(d-b)]t} \quad (6.1)$$

Consider dR in serial and integrate on x direction:

$$\begin{aligned} R &= \int_{x_1}^{x_2} \rho \frac{dx}{[(c-a)x+(d-b)]t} \\ &= \frac{\rho}{(c-a)t} \ln[(c-a)x+(d-b)] \Big|_{x_1}^{x_2} \\ &= \frac{\rho}{(c-a)t} \ln \frac{(c-a)x_2+(d-b)}{(c-a)x_1+(d-b)} \\ &= \frac{\rho}{(c-a)t} \ln \frac{(c-a)(x_1+h)+(d-b)}{(c-a)x_1+(d-b)} \end{aligned}$$

Assume $x_1 = 0$ to have

$$R = \frac{\rho}{(c-a)t} \ln \frac{(c-a)h+(d-b)}{(d-b)} \quad (6.2)$$

Define L_1 and L_2 to represent the length of the two parallel sides where $(d - b) = L_1$ and

$(c - a) = \frac{L_2 - L_1}{h}$, and as indicated before that h is the height, then

$$R = \frac{\rho h}{(L_2 - L_1)t} \ln \frac{L_2}{L_1} \quad (6.3)$$

6.3.1.2 Definition for Sensitivity

Based on the definition of resistance (6.3) and for isotropic linear elastic material

$$R = \frac{\rho h}{(l_2 - l_1)t} \ln \frac{l_2}{l_1} \quad (6.4)$$

Where l_1 and l_2 are constants. So

$$R = \left(\frac{\ln(l_2/l_1)}{l_2 - l_1} \right) \cdot \frac{\rho h}{t} \quad (6.5)$$

$$\frac{dR}{R} = \left(\frac{d\rho}{\rho} + \frac{dh}{h} - \frac{dt}{t} - \frac{dl}{l} \right) \cdot L \quad (6.6)$$

Where $L = \left(\frac{\ln(l_2/l_1)}{l_2 - l_1} \right)$ is a constant.

Still considering uniaxial tension on the x direction: $\frac{dt}{t} = \frac{dl}{l} = -\nu \frac{dh}{h}$, ν is the poisson's

ratio and $\frac{dl}{l} = \varepsilon_{axial}$

$$\frac{dR}{R} = \left(\frac{d\rho}{\rho} + (1 + 2\nu) \frac{dl}{l} \right) L \quad (6.7)$$

So the Gauge factor for a trapezoid shape sensor is:

$$\frac{dR/R}{\varepsilon_{axial}} = L \left(\frac{d\rho/\rho}{\varepsilon_{axial}} + (1 + 2\nu) \right) \quad (6.8)$$

Comparing the equation (6.8) with the equation (3.6): $\frac{dR/R}{\varepsilon_{axial}} = 1 + 2\nu + \frac{d\rho/\rho}{\varepsilon_{axial}}$, the

difference is (6.8) have the factor L which is determined by the size of the two parallel size. So by changing the L, it is possible to increase the sensitivity of the sensor.

6.3.2 Ring

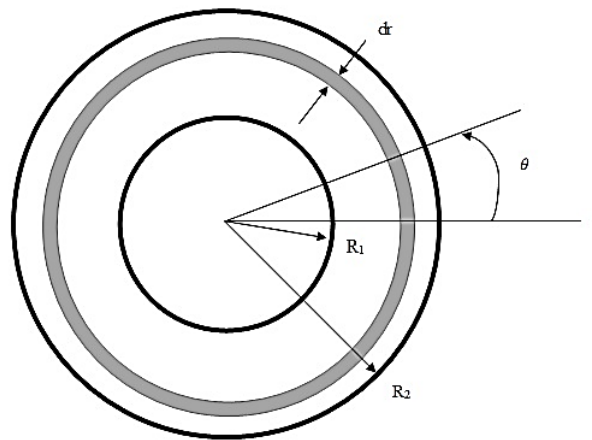


Figure 6.3 Sector and Ring

6.3.2.1 Definition for Resistance

For a sector with angle θ

$$dR = \rho \frac{dr}{r \cdot \theta \cdot t} \quad (6.9)$$

Integrate on r direction considering dR in serial:

$$R = \frac{\rho}{t \cdot \theta} \int_{R1}^{R2} \frac{dr}{r} \quad (6.10)$$

$$R = \frac{\rho}{t \cdot \theta} \ln \frac{R2}{R1} \quad (6.11)$$

For a full ring with $\theta = 2\pi$,

$$R = \frac{\rho}{2\pi t} \ln \frac{R2}{R1} \quad (6.12)$$

Where t is the thickness, $R1$ and $R2$ are the inner and outer radius of the ring, and ρ is the resistivity of the material.

6.3.2.2 Definition for Sensitivity

For isotropic linear elastic material, assume $R2 = r \cdot r2$ and $R1 = r \cdot r1$, where r is the variable, and $r1$ and $r2$ are constants. Based on equation (6.12)

$$R = \frac{\rho}{t \cdot \theta} \ln \frac{r2}{r1} \quad (6.13)$$

$$\ln R = (\ln r2 / r1) \cdot (\ln \rho - \ln t - \ln \theta) \quad (6.14)$$

$$\frac{dR}{R} = (\ln r^2/r_1) \left(\frac{d\rho}{\rho} - \frac{dt}{t} - \frac{d\theta}{\theta} \right) \quad (6.15)$$

Given $\frac{dt}{t} = \varepsilon_z$, $\frac{d\theta}{\theta} = \varepsilon_\theta$ and $\frac{dr}{r} = \varepsilon_r$,

$$\frac{dR}{R} = (\ln r^2/r_1) \left(\frac{d\rho}{\rho} - \varepsilon_z - \varepsilon_\theta \right) \quad (6.16)$$

Generally, using Barlow's Equation, the stress found is σ_r , and the linearized Hook's Law doesn't apply in this case, but it has been proved that the change in resistance and pressure have a linear relationship between them. So the safe way to define the sensitivity of the ring shaped pressure sensor is direct relate the pressure with the resistance change:

$$\frac{\Delta R/R}{\Delta P} = \text{Sensitivity} \quad (6.17)$$

However, in this case, the ring is placed on the center of the channel, the deformation only vary on radius direction and the deformation on thickness direction $\varepsilon_z = -\nu\varepsilon_r$ and $\sigma_r = E\varepsilon_r$, so from

equation (6.12) to get

$$\frac{dR}{R} = \left(\frac{\ln r^2/r_1}{2\pi} \right) \left(\frac{d\rho}{\rho} + 2\nu\varepsilon_r \right) \quad (6.18)$$

$$\frac{dR/R}{\varepsilon_r} = \left(\frac{\ln r^2/r_1}{2\pi} \right) \left(\frac{d\rho/\rho}{\varepsilon_r} + 2\nu \right) \quad (6.19)$$

Define the gauge factor as $\frac{dR/R}{\varepsilon_r}$.

6.4 SENSITIVITY CALIBRATION

For rectangular and trapezoidal shaped transducer, the uniaxial tension is applied using the same testing system in section 3.4 while for ring shaped ones, system used in section 3.5 to apply pressure on the membrane and collect the impedance of the transducer under different pressure. The sensitivity of the transducer of each pattern can then be evaluated.

6.4.1 Results and Discussions

The impedance Cole-Cole plot of ring shaped sample testing is shown in Figure 6.4, and the sensitivities of the thin film of rectangle, trapezoid and ring shape are summarized in Figure 6.5.

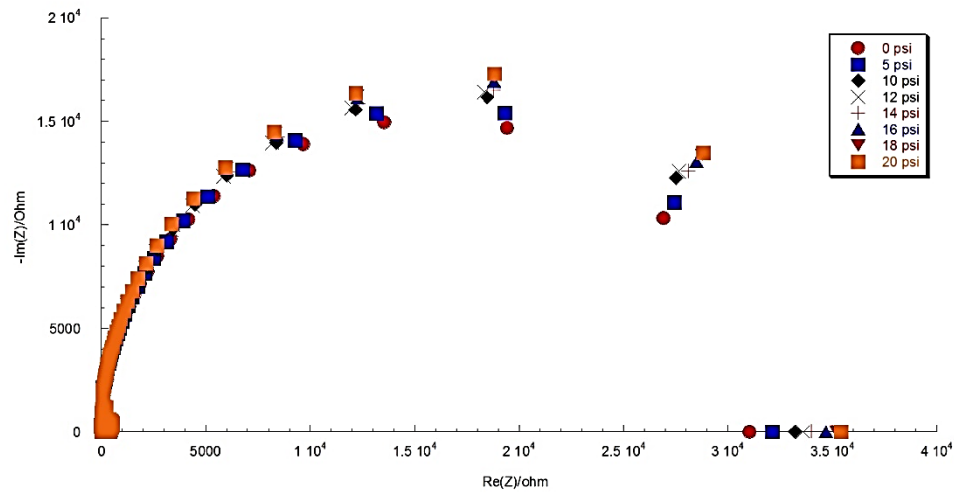


Figure 6.4 Impedance of Ring Shaped Transducer

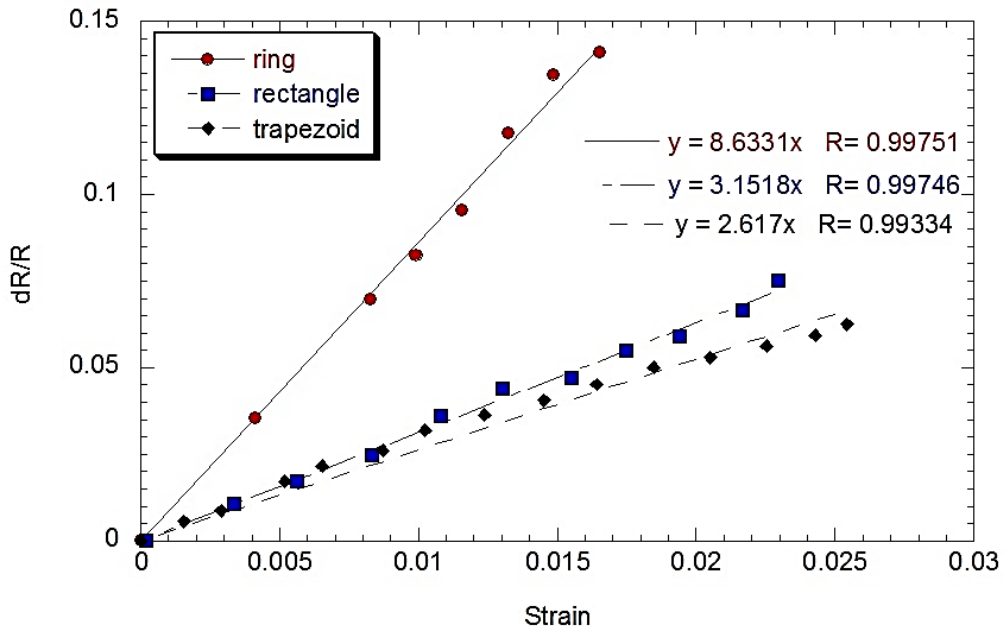


Figure 6.5 Sensitivity Summary

The difference of the sensitivity of rectangle and trapezoid can be proved by the definition of the gauge factor, that in this case the $h_2/h_1=2$ and the sensitivity of the trapezoid pattern is smaller than the one of the rectangle. However, the gauge factor of ring shaped isn't comparable with the other two because the different definition. But this result explains the different 'gauge factor' got from chapter 3 from two different testing method (i.e. tensile testing and pressure vessel).

7.0 CONCLUSIONS

7.1 PRINTING ADVANTAGES

Previous researchers utilize spin coating to fabricate the nanocomposite thin film on the polyimide substrate [6] or manually use transfer pipe or small brush to paint on the substrate [5]. Comparing to the traditional methods, inkjet printing method shows lots of advantages. Table 7.1 gives a brief summary to show the advantages. In the table, number 1, 2 and 3 are used to show ranks of each method in each specific aspect.

Table 7.1 Comparison of Different thin film Fabrication Methods

	Printing	Spin Coat	Painting
Material Efficiency	1	3	2
Geometry Control	1	3	2
Fabrication Speed	2	3	1
Repeatability	1	2	3
Flexibility	1	3	2
Easy for industrial usage	1	2	3

Utilizing printing methods makes almost zero material waste. Both drop size and the location of the drop on the substrate can be precisely controlled, which makes every drop of the material in use. While using spin coating, only less than one third of the dropped material stays on the substrate while rests are spread out. When painting manually, the drop size is so large that it is easy to flow around before the solvent evaporate, and that may also make non-uniform distribution of the material on the substrate. Also, the geometry of the thin film can be easily controlled. The thin film can be rectangular, circular or any kind of shape in need and the only thing need to do is to adjust the program in the printer controlling software. The resolution can be high, based on the lab condition, the size of the nozzle of printer head can be $60\ \mu\text{m}$ or $80\ \mu\text{m}$ which makes drop size around $80\ \mu\text{m}$ or $100\ \mu\text{m}$ respectively. Based on that, the thin film of nanocomposite can be small in size and it is possible to print on flexible substrate.

Due to the limitation of the printer used in this research, the printing process is tedious: it takes 30 min to print single layer of $15\text{mm} \times 1.5\text{mm}$ triangular with 2250 drops. Manually painting is the most practical choice in the lab, one can fabricate as many as specimens as possible. However, printing procedure can be speed up by using multi-print head printers or multi-nozzles print heads.

Printing method also shows great advantage in repeatability. Figure 7.1 shows the samples under SEM and optical microscope, both pictures shows that the distribution of the drops are uniform and have similar amount of carbon nanotube each drop. It suggests that samples with same geometry and similar CNT distribution can be repeated.

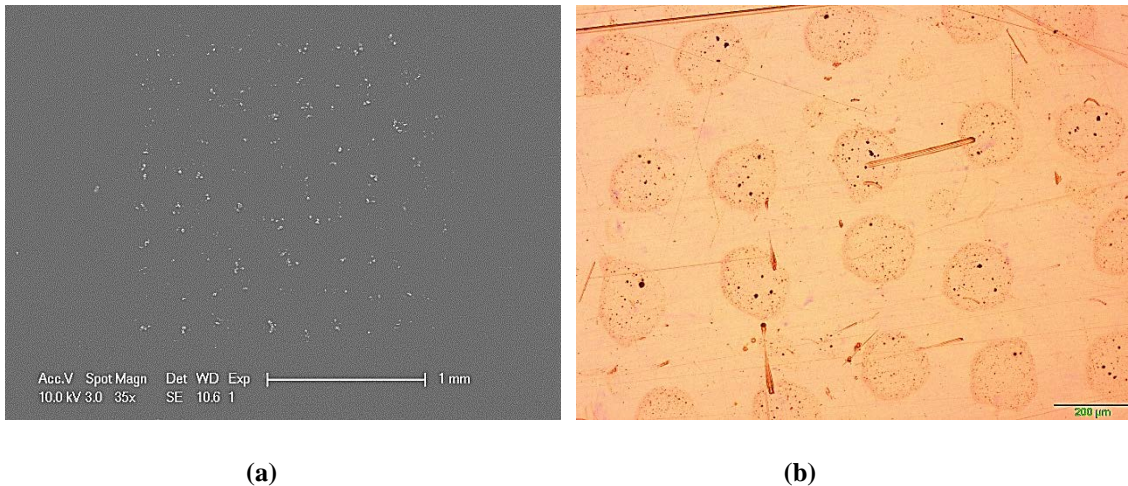


Figure 7.1 Photos of printed sample

7.2 CONCLUSIONS AND FUTURE WORKS

The main object of this research is to use inkjet printing method to fabricate CNT-PI nanocomposite thin film, and characterize its piezoresistive property for strain or pressure testing.

The CNT-PI nanocomposite with the best sensitivity was found by using tensile testing and pressure vessel. Using the tensile testing method, continuous uniaxial load was applied on the substrate and the DC resistance variations of different CNT weight ratio in the nanocomposite was monitored, and the gauge factors were calculated. In order to understand the electric property of the nanocomposite, impedance need to be tested, and one advantage of using pressure vessel is the impedance at some specific pressure level, in other words the transducer under specific strain, can be evaluated. The pressure on the transducer can be controlled and can be kept in a static state. Both the results from the two testing methods indicate the same CNT weight ratio of the nanocomposite should be the best choice for strain/pressure sensing, although

the 'gauge factor' got from the two testing method were not the same. The definition of the gauge factor seems to show that the gauge factor is a constant depend on the material property and the geometry change, however, simplifications were made when deriving the formula and the definition should be vary depending on different loading type and the different geometry of the transducer to achieve a more precise description of the piezoresistive property of the transducer. Using the same material, different patterns of the transducer were made. And considering the different possible application, the specific gauge factors of the transducers under specific kind of load were derived and experiments were conducted to calibrate the gauge factor. Considering the possible requirements for strain sensor for variable cross section, trapezoid shaped thin film were made, the experiment result showed the trapezoid shaped thin film can have a smaller gauge factor compare to a traditional rectangular transducer. However, it proved the mathematical formula that by changing the ratio of the two parallel edges, it is possible to have a gauge factor increment. The ring shaped should works best for pressure testing, especially the transducer is placed co-centered with the vessel and the ring has a small inner radius, the possible error on the gauge factor calculation caused by the un-uniform deformation on angular direction can be eliminated.

Temperature has giant effect on the performance of the piezoresistive strain/pressure sensing. The temperature coefficient of the nanocomposites were found, and it also shows that the 1.8wt% CNT-PI nanocomposite not only have a higher sensitivity of strain, but with lower sensitivity of temperature. Using the temperature coefficient, a dummy gauge can be used or a circuit can be added in the testing Wheatstone bridge to compensate the temperature effect. Humidity also could affect the performance of the transducer, and the parylene coating can effectively eliminate this affection.

When considering the humidity effect on the performance of the thin film, only the resistance change with humidity was tested. However, the gauge factor of the thin film under different humidity should be tested in the future. That will show how the performance of the transducer can be effected by the humidity and the right amount of parylene coating should be evaluated to eliminate the effect without intervene the mechanical performance of the thin film.

From this research, the gauge factor or sensitivity of the CNT-PI nanocomposite strain/pressure sensor are around 3 to 8, which don't show dominant advantage over other possible semiconductor nanocomposite strain gauge. Graphene-PI nanocomposites have shown a much higher gauge factor but due to the limitation of the thin film fabrication method, there are few consistent gauge factor reported. The inkjet printing technique has shown several advantages in building more uniform nanocomposite thin layer and in controlling the pattern geometry. It is possible to characterize the piezoresistive property of Graphene-PI nanocomposites with the inkjet printing method.

BIBLIOGRAPHY

- [1] Alciatore, David G., Michael B. Hestand, and David G. Alciatore. *Introduction to mechatronics and measurement systems*. Tata McGraw-Hill Education, 2007.
- [2] Kon, Stanley, Kenn Oldham, and Roberto Horowitz. "Piezoresistive and piezoelectric MEMS strain sensors for vibration detection." In *The 14th International Symposium on: Smart Structures and Materials & Nondestructive Evaluation and Health Monitoring*, pp. 65292V-65292V. International Society for Optics and Photonics, 2007.
- [3] Wang, H., Q. M. Zhang, L. E. Cross, R. Ting, C. Coughlin, and K. Rittenmyer. "The origins of electromechanical response in polyurethane elastomers." In *Applications of Ferroelectrics, 1994. ISAF'94., Proceedings of the Ninth IEEE International Symposium on*, pp. 182-185. IEEE, 1991.
- [4] Pelrine, Ronald E., Roy D. Kornbluh, and Jose P. Joseph. "Electrostriction of polymer dielectrics with compliant electrodes as a means of actuation." *Sensors and Actuators A: Physical* 64, no. 1 (1998): 77-85.
- [5] Chen, Qian, Yingying Sun, Ying Wang, Hongbin Cheng, and Qing-Ming Wang. "ZnO nanowires–polyimide nanocomposite piezoresistive strain sensor." *Sensors and Actuators A: Physical* 190 (2013): 161-167.
- [6] Wang, Yizhong, Allen X. Wang, Ying Wang, Minking K. Chyu, and Qing-Ming Wang. "Fabrication and characterization of carbon nanotube–polyimide composite based high temperature flexible thin film piezoresistive strain sensor." *Sensors and Actuators A: Physical* 199 (2013): 265-271.
- [7] Kang, Inpil, et al. "A carbon nanotube strain sensor for structural health monitoring." *Smart materials and structures* 15.3 (2006): 737.
- [8] Hu, Ning, Yoshifumi Karube, Masahiro Arai, Tomonori Watanabe, Cheng Yan, Yuan Li, Yaolu Liu, and Hisao Fukunaga. "Investigation on sensitivity of a polymer/carbon nanotube composite strain sensor." *Carbon* 48, no. 3 (2010): 680-687.
- [9] Wang, Yizhong, Minking K. Chyu, and Qing-Ming Wang. "Passive wireless surface acoustic wave CO₂ sensor with carbon nanotube nanocomposite as an interface layer." *Sensors and Actuators A: Physical* 220 (2014): 34-44.

- [10] Hsieh, Gen-Wen, Flora M. Li, Paul Beecher, Arokia Nathan, Yiliang Wu, Beng S. Ong, and William I. Milne. "High performance nanocomposite thin film transistors with bilayer carbon nanotube-polythiophene active channel by ink-jet printing." *Journal of applied physics* 106, no. 12 (2009): 123706.
- [11] Chen, Pochiang, Haitian Chen, Jing Qiu, and Chongwu Zhou. "Inkjet printing of single-walled carbon nanotube/RuO₂ nanowire supercapacitors on cloth fabrics and flexible substrates." *Nano Research* 3, no. 8 (2010): 594-603.
- [12] Loffredo, F., A. D. G. D. Mauro, G. Burrasca, V. La Ferrara, L. Quercia, E. Massera, G. Di Francia, and D. Della Sala. "Ink-jet printing technique in polymer/carbon black sensing device fabrication." *Sensors and Actuators B: Chemical* 143, no. 1 (2009): 421-429.
- [13] Simmons, Jr Edward E. "Explosion pressure gauge." U.S. Patent 2,327,935, issued August 24, 1943.
- [14] Ruge, Arthur C. "Strain gauge." U.S. Patent 2,350,972, issued June 6, 1944.
- [15] Figliola, Richard S., and Donald E. Beasley. "Theory and design for mechanical measurements." *Measurement Science and Technology* 12, no. 10 (2001): 1743.
- [16] http://en.wikipedia.org/wiki/Strain_gauge
- [17] Micro-Measurement Division, Vishay Precision Group, Inc., *Strain Gage Selection: Criteria, Procedures, Recommendations*, Technical Note 505-4, Malvern, PA, 2014.
- [18] Micro-Measurement Division, Vishay Precision Group, Inc., *Strain Gage Rosettes: Selection, Application and Data Reduction*, Technical Note 515, Malvern, PA, 2014.
- [19] Micro-Measurement Division, Vishay Precision Group, Inc., *Design Considerations for Diaphragm Pressure Transducers*, Technical Note 515, Malvern, PA, 2010.
- [20] Micro-Measurement Division, Vishay Precision Group, Inc., *Errors Due to Transverse Sensitivity in Strain Gages*, Technical Note 509, Malvern, PA, 2011.
- [21] He, Rongrui, and Peidong Yang. "Giant piezoresistance effect in silicon nanowires." *Nature nanotechnology* 1, no. 1 (2006): 42-46.
- [22] Reck, Kasper, Jacob Richter, Ole Hansen, and Erik Vilain Thomsen. "Piezoresistive effect in top-down fabricated silicon nanowires." In *Micro Electro Mechanical Systems, 2008. MEMS 2008. IEEE 21st International Conference on*, pp. 717-720. IEEE, 2008.
- [23] Wan, Qing, Q. H. Li, Y. J. Chen, Ta-Hung Wang, X. L. He, J. P. Li, and C. L. Lin. "Fabrication and ethanol sensing characteristics of ZnO nanowire gas sensors." *Applied Physics Letters* 84, no. 18 (2004): 3654-3656.

- [24] Yu, Xun, and Eil Kwon. "A carbon nanotube/cement composite with piezoresistive properties." *Smart Materials and Structures* 18, no. 5 (2009): 055010.
- [25] Kiuchi, Mario, Shinji Matsui, and Yoshitada Isono. "The piezoresistance effect of FIB-deposited carbon nanowires under severe strain." *Journal of Micromechanics and Microengineering* 18, no. 6 (2008): 065011.
- [26] Loh, Kenneth J., Jerome P. Lynch, B. S. Shim, and N. A. Kotov. "Tailoring piezoresistive sensitivity of multilayer carbon nanotube composite strain sensors." *Journal of Intelligent Material Systems and Structures* 19, no. 7 (2008): 747-764.
- [27] Chen, Qingyun, Yuezhen Bin, and Masaru Matsuo. "Characteristics of ethylene-methyl methacrylate copolymer and ultrahigh molecular weight polyethylene composite filled with multiwall carbon nanotubes prepared by gelation/crystallization from solutions." *Macromolecules* 39, no. 19 (2006): 6528-6536.
- [28] Wichmann, Malte HG, Samuel T. Buschhorn, Jan Gehrmann, and Karl Schulte. "Piezoresistive response of epoxy composites with carbon nanoparticles under tensile load." *Physical Review B* 80, no. 24 (2009): 245437.
- [29] Chang, Fuh-Yu, Ruoh-Huey Wang, Hsiharng Yang, Yu-Hsien Lin, Tse-Min Chen, and Shu-Jiuan Huang. "Flexible strain sensors fabricated with carbon nano-tube and carbon nano-fiber composite thin films." *Thin Solid Films* 518, no. 24 (2010): 7343-7347.
- [30] Kim, Young-Ju, Ju Young Cha, Heon Ham, Hoon Huh, Dae-Sup So, and Inpil Kang. "Preparation of piezoresistive nano smart hybrid material based on graphene." *Current Applied Physics* 11, no. 1 (2011): S350-S352.
- [31] Hu, Ning, Hisao Fukunaga, Satoshi Atobe, Yaolu Liu, and Jinhua Li. "Piezoresistive strain sensors made from carbon nanotubes based polymer nanocomposites." *Sensors* 11, no. 11 (2011): 10691-10723.
- [32] Bessonov, Michael I., and Vladimir A. Zubkov. *Polyamic acids and polyimides: synthesis, transformations, and structure*. CRC Press, 1993.
- [33] Wijshoff, Herman. "The dynamics of the piezo inkjet printhead operation." *Physics reports* 491.4 (2010): 77-177.
- [34] Le, Hue P. "Progress and trends in ink-jet printing technology." *Journal of Imaging Science and Technology* 42.1 (1998): 49-62.
- [35] Sweet, Richard G. "High frequency recording with electrostatically deflected ink jets." *Review of scientific instruments* 36.2 (1965): 131-136.
- [36] Taylor, Geoffrey. "Disintegration of water drops in an electric field." *Proceedings of the Royal Society of London. Series A. Mathematical and Physical Sciences* 280.1382 (1964): 383-397.

- [37] Bugdayci, Nur, David B. Bogy, and Frank E. Talke. "Axisymmetric motion of radially polarized piezoelectric cylinders used in ink jet printing." *IBM Journal of Research and Development* 27.2 (1983): 171-180.
- [38] Stemme, Erik, and S-G. Larsson. "The piezoelectric capillary injector—a new hydrodynamic method for dot pattern generation." *Electron Devices, IEEE Transactions on* 20.1 (1973): 14-19.
- [39] Kyser, Edmond L., Leland F. Collins, and Nick Herbert. "Design of an impulse ink jet." *Journal of Applied Photographic Engineering* 7.3 (1981): 73-79.
- [40] Calvert, Paul. "Inkjet printing for materials and devices." *Chemistry of materials* 13.10 (2001): 3299-3305.
- [41] Kaydanova, Tanya, et al. "Direct-write inkjet printing for fabrication of barium strontium titanate-based tunable circuits." *Thin Solid Films* 515.7 (2007): 3820-3824.
- [42] Van Osch, Thijs HJ, et al. "Inkjet printing of narrow conductive tracks on untreated polymeric substrates." *Advanced Materials* 20.2 (2008): 343-345.
- [43] Rausch, Jacqueline, et al. "Printed piezoresistive strain sensors for monitoring of light-weight structures." (2011).
- [44] Hu, Ning, Yoshifumi Karube, Cheng Yan, Zen Masuda, and Hisao Fukunaga. "Tunneling effect in a polymer/carbon nanotube nanocomposite strain sensor." *Acta Materialia* 56, no. 13 (2008): 2929-2936.
- [45] MicroFab Techniques, Inc., *Jetlab Technical Reference Manual*, Plano, Texas, 2007.
- [46] MicroFab Techniques, Inc., *Jetlab Tutorial Guide*, Plano, Texas, 2006.